Energy & Environmental Science

Dynamic Article Links

Cite this: *Energy Environ. Sci.*, 2012, **5**, 5510

www.rsc.org/ees

REVIEW

Resonant levels in bulk thermoelectric semiconductors

Joseph P. Heremans,*[ab] Bartlomiej Wiendlocha[ac] and Audrey M. Chamoire[a]

Received 7th September 2011, Accepted 17th October 2011
DOI: 10.1039/c1ee02612g

Distortions of the electronic density of states (DOS) are a potent mechanism to increase the thermopower of thermoelectric semiconductors, thereby increasing their power factor. We review band-structure engineering approaches that have been used to achieve this, resonant impurity levels, dilute Kondo effects, and hybridization effects in strongly correlated electron systems. These can increase the thermoelectric power of metals and semiconductors through two mechanisms: (1) the added density of states increases the thermopower in a nearly temperature-independent way; (2) resonant scattering results in a strong electron energy filtering effect that increases the thermopower at cryogenic temperatures where the electron–phonon interactions are weaker. Electronic structure calculation results for Tl:PbTe and Ti:PbTe are contrasted and identify the origin of the thermopower enhancement in Tl:PbTe. This leads to a discussion of the conditions for DOS distortions to produce thermopower enhancements and illustrates the existence of an optimal degree of delocalization of the impurity states. The experimentally observed resonant levels in several III–V, II–VI, IV–VI and V_2-VI_3 compound semiconductor systems are reviewed.

Introduction

Great progress has been made in the last decade toward increasing the thermoelectric figure of merit zT in thermoelectric semiconductors. The central problem is that zT consists of a set of mutually "counter-indicated" materials properties, namely the thermopower (or Seebeck coefficient), S, and the electrical (σ) and thermal (κ) conductivities of the material. The label "counter-indicated" means that most mechanisms that improve one also are deleterious to the other. Explicitly, we can write zT as the product of two sets of these counter-indicated properties shown here in parentheses:

$$zT \equiv \frac{S^2\sigma}{\kappa}T = \left(S^2 n\right)\left(\frac{\mu}{\kappa}\right)qT \quad (1)$$

whereby we have written the electrical conductivity as $\sigma = nq\mu$, with n the charge carrier concentration, q its charge and μ its mobility. The ratio (μ/κ) is counter-indicated because defects and impurities that affect one of these properties usually also affect the other. The other counter-indicated property is the product (S^2n): indeed, it is a general rule in doped semiconductors and metals that the higher the carrier concentration, the lower the thermopower, a relation attributed to Mr. N. L. Pisarenko in the seminal monograph on thermoelectricity by Abram Ioffe.[1,2]

Most work in the last decade focused on improving the ratio (μ/κ) by reducing the lattice part of the thermal conductivity using phonon scattering mechanisms, such as nanostructures or localized phonon modes, that have a relatively smaller effect on scattering electrons; this approach has been reviewed elsewhere.[3] Slack[4] teaches us that there is a limit to the improvement in zT that can be achieved this way, because the phonon conductivity is limited in most bulk systems to what is known as the amorphous limit, *i.e.* where the phonon mean free path is on the order of one

[a]*Department of Mechanical and Aerospace Engineering, The Ohio State University, Columbus, Ohio, USA 43210*
[b]*Department of Physics, The Ohio State University, Columbus, Ohio, USA 43210*
[c]*AGH University of Science and Technology, Faculty of Physics and Applied Computer Science, al. A. Mickiewicza 30, 30-059 Krakow, Poland*

Broader context

Thermoelectric materials are useful in all-solid-state conversion between heat and electrical power. The technology is most promising in waste-heat recovery applications, where its extreme reliability and high power density makes it the prime choice in mobile applications. Research during the last decade has resulted in a near-doubling of the conversion efficiency, characterized by the figure of merit zT, mostly through the reduction of the lattice thermal conductivity. One complementary technology that promises to enhance the thermoelectric power instead is the use of "resonant impurities" as dopants. What those dopants are, and how they work, is reviewed here.

This journal is © The Royal Society of Chemistry 2012

interatomic distance. Comparatively less research effort has been aimed at increasing the thermoelectric power factor $P = S^2\sigma$, or more specifically the product (S^2n), and that quantity is the object of the present review.

The product (S^2n) is a purely electronic property, dominated by the details of the electronic band structure and of the scattering mechanisms. Therefore, one approach to increase (S^2n) is by engineering distortions of the electronic density of states (DOS) near the Fermi energy. Because thermoelectric technology can only be expected to impact the world energy issues if it can convert large amounts of thermal and electrical power, we concentrate here on approaches that apply to bulk three-dimensional thermoelectric materials. This review is organized in five sections.

(1) In the first section, the mechanisms that can be used to distort the DOS in bulk solids will be briefly described, and the relations between them put in perspective.

(2) The second section focuses on the physical origin and nature of resonant impurity levels, sometimes called virtual bound states. These levels create distortions of the DOS. Their wavefunctions can be more atom-like ("localized states") or more free-electron-like ("extended states"). The geometrical scale of this degree of "extension" is the volume occupied by an atom in the lattice, or the interatomic distance (the Ioffe-Regel rule).

(3) The third section reviews the Mott relation in its general form, and shows how and under what conditions distortions of the DOS lead to an enhanced thermopower and thermoelectric figure of merit.

(4) In the fourth section, we review the literature on existing resonant levels in semiconductors. The experimental data on thermoelectric semiconductors based on PbTe, used for power generation applications near 500 °C, and based on Bi_2Te_3 used for cooling applications near room temperature are discussed in detail.

(5) The fifth section describes Density Functional Theory (DFT) band structure calculations for two cases, Tl:PbTe and Ti:PbTe, showcasing the contrast between more localized and more extended resonant levels.

1. Distortions of the density of states

The density of states (DOS), $g(E)$ in units of number of states per eV per cm^{-3} of material, is a measure of how many electron states are available in a unit volume of solid at energies between E and $E + dE$. Mathematically, $g(E)$ is the function that enables the transformation of variables in the calculation of the transport integrals, from integrals of the type $\frac{1}{4\pi^3}\iiint_{E\le E_0} F(\mathbf{k})d^3\mathbf{k}$ over momentum-space (**k**-space) defined in a Brillouin zone of a three-dimensional (3-D) solid, to scalar integrals of the type $\int_0^{E_0} F(E)g(E)dE$ over energy E (here $F(E)$ is an arbitrary function).

The DOS including spin degeneracy, in 3-D is defined by[5]

$$g(E) \equiv \frac{1}{4\pi^3}\iint_S \frac{dS}{|\nabla_k E(\mathbf{k})|} \quad (2)$$

where S denotes the equi-energy surface of energy E. The dimensionality of the system is of primary importance in determining the shape of the integrals. For a quasi-free three-dimensional (3-D) electron with a quadratic dispersion relation $E(\mathbf{k})$, $g(E) \propto \sqrt{E}$. In a 2-D electron system, $g(E)$ consists of a series of steps at quantized energy levels E_N ($N = 1, 2\ldots$). In a 1-D quantum wire, $g(E)$ has divergent maxima shaped like $g(E) \propto 1\Big/\sqrt{(E - E_{N_1,N_2})}, E \ge E_{N_1,N_2}$ at quantized energies

Joseph P. Heremans

Dr Joseph P. Heremans is Professor of Mechanical and Aeronautical Engineering, and of Physics, at the Ohio State University, where he holds a chair as Ohio Eminent Scholar. His research focuses on the physics of narrow-gap semiconductors and semimetals, and particularly on thermal, electronic and thermoelectric transport properties. Most recently, he initiated the study of the thermal transport properties of spin currents (the spin-Seebeck effect).

Bartlomiej Wiendlocha

Dr Bartlomiej Wiendlocha is currently Adjunct Professor at the AGH University of Science and Technology in Krakow, Poland. He obtained his PhD in Physics from AGH-UST in 2009. He joined Joseph P. Heremans' group in 2011 as a postdoctoral researcher, now continues collaboration as a visiting scientist. He is interested in theoretical solid state physics, focusing on first principles calculations of electronic structure, superconducting, magnetic and thermoelectric properties.

Audrey M. Chamoire

Dr Audrey Chamoire is currently a postdoctoral researcher in Joseph P. Heremans' group in the department of Mechanical Engineering at the Ohio State University. Her research focuses on synthesis, characterization, and transport properties measurements of rare earth based thermoelectric materials. She recently initiated a study of hybrid organic/inorganic semiconductor materials for thermoelectric conversion of heat.

$E_{N1,N2}$ ($N1$, $N2 = 1, 2\ldots$). For the 3-D case that concerns this review, we will derive further how S depends on $g(E = E_F)$ in a general way, where E_F is the Fermi energy. For a first introduction to the subject, it is sufficient to state Mahan and Sofo's[6] conclusion: the larger g and the stronger its dependence on E, the higher $S(n)$ will be for a given carrier concentration. The limiting case, where $g(E)$ is a delta function at 2.4 k_BT above or below E_F, is shown to give the optimal zT enhancement. Of course this is unattainable in nature because local variations in sample composition would broaden such a delta function. A second limitation is the presence of available electronic states due to atoms other than the ones that create the delta-function-like DOS in the solid, defined here as the "background DOS". Mahan and Sofo demonstrate that this background DOS strongly decreases the optimal zT, but a non-zero background DOS is indispensable to control the position of E_F. The goal of research on the thermoelectric power factor is therefore to distort and increase g as much as possible over and above a $E^{1/2}$ function near the Fermi level. Hicks and Dresselhaus[7] predict that 2-D quantum wells and 1-D quantum wires could make excellent thermoelectric materials, based on the shape of $g(E)$ outlined above; the experimental work based on such effects is quite promising and was also reviewed previously.[8]

For the sake of clarity, we categorize in this review the approaches used to distort the DOS in bulk solids into four somewhat arbitrary classes, summarized in Fig. 1: a) two-band structures (2B), b) resonant levels (RL) also known as virtual bound states, c) hybridization gaps (HG), also known as Kondo gaps and d) dilute Kondo alloys (DK). Obviously, two-band structures are not properly "distortions" of the DOS, as they are inherent from the dispersion relation of the solid; nevertheless, it has long been known that they can lead to impressive values of the thermopower and of zT. Classes RL, DK and HG are related,

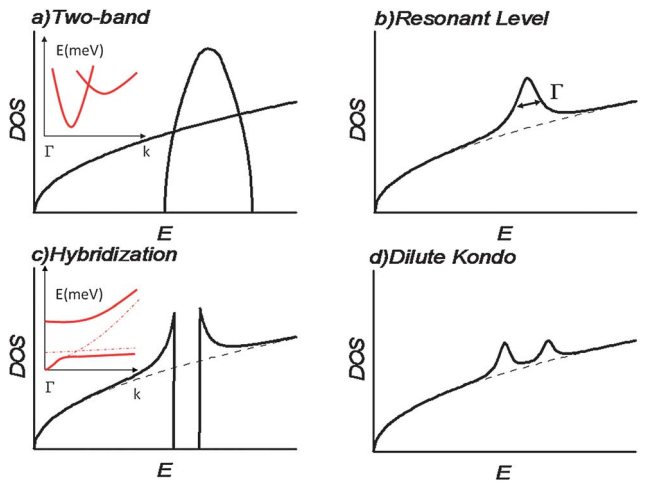

Fig. 1 Mechanisms used to distort the density of states in solids and to increase their thermopower. Two-band conduction is not properly a "distortion", but can lead to a large thermopower. Resonant impurity levels, which do not involve a magnetic exchange between the impurity and the host solid, are closely related to Kondo systems, though the latter involve dilute magnetic impurities. Systems with band hybridization are observed in systems in which the magnetic atoms are major constituents, and here the coupling opens a Kondo gap.

as we will show. Both DK and HG classes concern systems in which atoms with electrons on d-level or f-level are added to conventional semiconductors with bands dominated by s or p levels, but they differ in concentration: DK concerns dilute alloys, HG concentrated alloys and intermetallic compounds. Resonant levels, in contrast, do not necessarily involve d-levels, but can arise from s and p-levels, especially in semiconductors. The name of Jun Kondo is often associated with all correlated systems of classes DK and HG which involve magnetic ions, though it is the dilute alloys that were the object of his pioneering early work.[9]

Both RL and DK systems were studied first in metals. RL's were discovered first in atomic physics, then adapted to solid state physics in 1953 by Korringa and Gerritsen[10] and in 1956 by Friedel.[11] RL's involve a coupling between electrons on a dilute impurity and those in the conduction or the valence band of the host solid, while in DK systems a magnetic contribution is added to that interaction. Resonant levels will be treated in some detail in the next section, and we will conclude this section with a brief description of DK and HG system.

The first signature of a DK system in a metal is a non-monotonic temperature dependence of the resistivity. The resistivity ρ of a pure metal decreases monotonically with temperature following the "Bloch-Grüneisen" or "Bloch-T^5" law,[5] which holds when boundary and acoustic phonon scattering of the charge carriers dominate. According to the Bloch-Grüneisen law, at the lowest temperature, the electron mean free path (mfp) is dominated by scattering on grain boundaries and defects, and, since the carrier density does not change with temperature in metals, the resistivity is constant, $\rho \sim T^0$ At slightly higher temperatures, where phonon scattering starts dominating, but below the Debye temperature, so that the number of phonons and the electron–phonon scattering angles are strong functions of T, one observes $\rho \sim T^5$. Above the Debye temperature, metals show $\rho \sim T^1$. When small amounts of transition metal impurities (Fe, Cr, Mn…) are added to Cu, Ag or Au, clear deviations were observed from the Bloch-Grüneisen law. The first effects were observed in very dilute alloys at temperatures near where the pure host metal's resistivity had its transition between the T^5 and T^0 laws. In these dilute alloys (*e.g.* of ppm's of Fe in Au), $\rho(T)$ was observed to no longer be monotonic in T, going through a minimum near a characteristic "Kondo" temperature T_K, and then increasing again as the temperature is lowered below T_K. Later on, systems were identified in which T_K falls at a much higher temperature, in the T^5 or even the T^1 regime. The thermopower, which is normally (*i.e.* excluding phonon drag) proportional to T in metals, is greatly enhanced following a Gaussian peak in log(T) centered on T_K in the alloys that show a minimum in resistivity. Kondo explained the effect in 1964[9] by realizing that conduction electrons may change their spin states when they scatter on magnetic impurities. The DK signature in transport is based on an elaborate energy-dependence of the scattering probabilities. Here, Kondo considers not only the commutation relations between the creation and annihilation operators in calculating the matrix elements of the interactions, but also the spin raising and spin lowering operators. This mechanism is inherently a three-step scattering effect based on applying the Pauli exclusion principle to an intermediate state where an internal degree of freedom of the scatterer, namely its

 This journal is © The Royal Society of Chemistry 2012

spin, is involved. Following Blatt *et al.*[12] we represent the DOS in DK alloys as similar to that of the resonant levels, but with a magnetic splitting of the excesses in the DOS into a spin-up and a spin-down bump. These states do influence transport through scattering, and the Fermi level lies in between the two bumps in Fig. 1(d) (DK). T_K can reach above 1000 K,[13] but the amplitude of the peak in S rarely exceeds a few tens of $\mu V\ K^{-1}$ in practice.[14]

Considering now the frame labeled hybridization in Fig. 1(c), this can be viewed as a limiting case of the DK situation, where the magnetic atoms become a major constituent in the solid, so that their electronic levels contribute in a major way to the band structure. When a nearly dispersion-less energy band that originates from the *d* or *f* levels of a rare-earth or transition metal constituent intersects a band with *sp* character in a semiconductor or metal, those two can hybridize.[15] A hybridization gap then opens in the DOS as depicted in Fig. 1, and the local DOS near the gap is strongly distorted. Because they are based on similar Kondo interactions, but have an energy gap, they are sometimes called Kondo insulators. Examples of classical Kondo insulators are CeNiSn, $CePd_3$ and $Ce_3Bi_4Pt_3$,[16] and it is possible that hybridization may play a role in the extraordinarely high thermopowers of semiconductors like $FeSb_2$[17] (although other mechanisms are possible or can contribute[18]) and metals like $YbAl_3$.[19] Many decades of research in this field have shown that hybridization gaps are not easy to use in the design of thermoelectric materials, particularly when they involve 4*f*-levels. Indeed, these typically form very flat bands in k-space which promise a large enhancement in $g(E)$ and thus in thermopower,[6] but create difficulties in attempts to optimize the location of E_F in the *f*-level band. In the elemental rare-earth metals it is sometimes suggested (there are few experimental data) that the *f*-levels tend to split into two broad (in k-space) high-DOS bands, typically one several eV above and one several eV below the Fermi energy.[5] It is possible that some semiconducting rare earth compound will be proven to be an excellent thermoelectric based on the properties of its 4*f* electrons, but an additional difficulty in discovering such a system arises from the fact that binary or ternary phase diagrams show very few solid solution regions in rare-earth pnictides or chalcogenides, which tend to form intermetallics in which E_F is hard to tune chemically.

For completeness, we mention that distortions of the DOS or effective mass enhancements, as well as strong enhancements of the thermopower, can also be induced by electron–phonon interactions. In this category fit such effects as phonon-drag,[20] the Nielsen-Taylor pseudo-phonon drag effect,[21] and polaron mass enhancements.[22] Very intuitively, the enhancement of the effective mass that accompanies electron–phonon interactions, particularly the polaron effect, can be described as follows. When an electron exerts a force on the neighboring atoms sufficient to excite a phonon, it drags a mechanical displacement of the lattice atoms away from their equilibrium positions alongside its path. In polaron conduction, the distortion of the position of the atoms moves alongside the electron, strongly slowing down its group velocity dE/dk. This results in a distortion of the electron dispersion relation and a local increase in effective mass. Such effects are measurable in the electronic specific heat and in the thermopower, but since we know of no example where they resulted in an increase in zT yet, we refer the reader to a more in-depth review[23] for quantitative explanations. In general, we expect scattering and electron–phonon interaction effects to be more useful in thermoelectric materials designed to operate at cryogenic temperatures, where classical electron–phonon scattering is minimized. This section contained only cursory descriptions of possible ways to enhance the DOS, in order to provide an overall context for the next section on resonant levels.

2. Resonant levels (RL's)

Resonant impurities have been shown to increase the thermoelectric figure of merit of technologically important thermoelectric compound semiconductors, such as are used in electrical power generation (IV–VI compounds, such as based on PbTe) or Peltier cooling (V_2-VI_3 compounds, such as based on Bi_2Te_3). The two resonant impurities that enhance thermopower in these are thallium in the valence band of PbTe[24] and tin in the valence band of Bi_2Te_3.[25] As outlined above, resonant impurities are a concept introduced in solid state physics for metals first, but they do exist in many semiconductors: older reviews were published by Nemov[26] and Volkov.[27]

Consider first (Fig. 2, which shows an "empty" conduction band before the Fermi level is determined) the classical case of a donor impurity in a semiconductor, such as P in Si. Phosphorous atoms share four electrons with the neighboring Si atoms, leaving one extra electron that remains weakly bound to the P. An energy E_D (~a few meV, equivalent to a small thermal excitation energy, for conventional dopants in conventional semiconductors) is sufficient to overcome the bond between the P atom and its 5th electron and to release that electron into the conduction band of the host material. This is analogous to the case of a 1*s* electron on the hydrogen atom in vacuum, which can be released by the addition of one Rydberg of energy. We label this the *hydrogenoid model*, and E_D is an *effective Rydberg* R^*. We depict the energy level of this 5th electron as lying E_D below the conduction band edge and in the energy gap of the semiconductor. In contrast, resonant donor impurities would have electronic energy levels for which E_D is negative, with the impurity level falling inside the conduction band and coinciding with energies of extended states (see Fig. 2). Friedel labeled this a "virtual bound state", also called a resonant state. Following Blatt *et al.*,[12] it is useful to think of the resonant level as a bound level with an energy that falls above to the conduction band (CB) edge or below the valence band (VB) edge. As this state has now

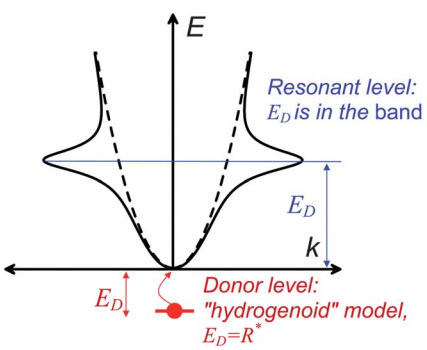

Fig. 2 Schematic representation of a conduction band, a hydrogenoid impurity, and a resonant impurity.

the same energy as an extended state, the two will resonate to build up two extended states of slightly different energies; these in turn will have the same energies as other extended states with whom they will resonate in turn, and so on. Consequently, the resonant state develops a certain width Γ. Both E_D and Γ are essential design parameters in optimizing zT, so that they warrant a further discussion, for which we will follow Daniel and Friedel.[28]

Since impurity atoms have multiple electron energy levels, some can be deeply bound, others weakly bound and yet others resonant. Fig. 3 shows schematically the potentials and energies experienced by electrons as they move over the periodically arranged nuclei of atoms in a solid. The band structure describes the effect of the periodic potential of the atoms of the host solid. The Hamiltonian of an electron of the host solid unperturbed by the impurity, H_0, has eigenvalues $H_0|\mathbf{k}> = E_\mathbf{k}|\mathbf{k}>$ describing electrons that reside in extended (plane-wave-like) states, at an energy $E(\mathbf{k})$ with a quantum number that is their wavevector **k.** In the spatial vicinity of the impurity, there is a disturbance of the periodic potential, on average by an amount V which is the perturbation energy. Let us write the Hamiltonian of the unperturbed impurity as having (atom-like) eigenvalues E_0 and atomic quantum numbers O: $H_0|O> = E_0|O>$. In practice, O is the orbital quantum number L of the impurity electron. Depending on the parameters, E_0 can correspond to either a bound state, or to an extended state. If it is an extended state, E_0 will fall in the conduction or valence band of the host semiconductor, where it resonates, which means that there is an interaction between the extended states (assumed of *s*-level character) of the host and the energy level of the impurity. Daniel and Friedel[28] assume the impurity energy level to be a *d*-level, as they consider cases such as Fe impurities in Au. The true

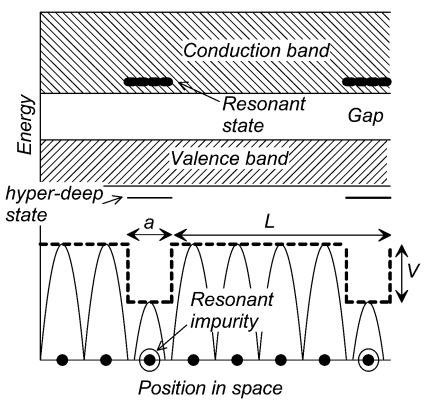

Fig. 3 Schematic energy *versus* distance diagram where the spheres on the bottom represent atoms. The periodic potential of the host atoms of the solid is experienced by conduction electrons and results in the formation of conduction and valence bands, extended states available to the nearly-free electrons. The resonant impurities perturb this potential, diffusing the nearly-free electrons over that area of the crystal, and creating a range of additional available energy levels, some bound (deep states inside the gap, or even hyper-deep states in the next gap below the valence band) and some at energies falling inside the extended states, here the conduction band. The figure represents schematically the case for In:PbTe, where the resonant states are in the conduction band.

Hamiltonian $H = H_0 + V$ takes into account the *s*-*d* interaction; its eigenstates ($|\Psi>$) are built of wavepackets from both the $|\mathbf{k}>$ extended states of the host solid and the $|O>$ of the impurity that are close to it in energy. Daniel and Friedel derive:

$$\begin{aligned} H|\psi\rangle &= (H_0 + V)|\psi\rangle = E|\psi\rangle \\ |\psi\rangle &= c|O\rangle + \iiint a(\mathbf{k})|\mathbf{k}\rangle d^3\mathbf{k} \end{aligned} \tag{3}$$

and solve this. The amount of impurity-induced $|O>$ state inside the state $|\Psi>$ is given by:

$$\begin{aligned} |c^2| &= \frac{|<O|V|\mathbf{k}>|^2}{(E - E_0 - \Delta)^2 + \left(\frac{\Gamma}{2}\right)^2} \\ \Gamma &= 2\pi\overline{|<O|V|\mathbf{k}>|^2}\, g(E) \end{aligned} \tag{4}$$

where Δ is an integral over the Brillouin zone of $|<O|V|\mathbf{k}>|^2$ and $g(E)$ is the DOS of the extended states of the host material. The resonant state can accommodate the total amount of charge initially included in the impurity. The amount of charge in the $|\mathbf{k}>$ states does not change either. Therefore, the extra electrons from the impurity have to be accommodated by the impurity-state $|O>$ contribution $|c|^2$ to the coupled state given by eqn (4). This contribution to the total $g(E)$ is a Lorentzian function of energy, as shown in Fig. 1, with a full width at half maximum Γ.

The explanation above makes it appear as if the $|\Psi>$ state is spatially concentrated near where the impurity is located, though it is mixed with extended states $|\mathbf{k}>$. This raises a conceptual difficulty: localized (atom-like) and extended (plane-wave-like) states cannot coexist at the same energy for a given configuration.[29] In liquid metals or in polaronic conductors this problem is avoided because the atomic configurations change near the charge carrier. In the present case the picture needs to be refined.

The refinement comes from the concept of Wigner delay time τ_W,[30] defined as the time spent by an electron at the resonant center. In scattering theory, it is related to the energy-dependent phase shift $\delta_O(E)$ the electron undergoes as it's wavefunction Ψ interferes with the impurity by $\tau_W = 2\hbar\frac{\partial\delta_O(E)}{\partial E}$, where O is the angular momentum index. The resonance occurs when the phase shift $\delta_O(E)$ changes from 0 to π over the energy interval Γ, preferably small on the scale of k_BT. The value of E_D is the energy where $\delta_O(E_D) = \pi/2$. Because $\delta_O(E)$ varies rapidly with energy in the vicinity of the resonance energy E_D, the time τ_W spent by the electron near the resonance center becomes long. The limiting cases are those of the free electron for which $\tau_W = 0$, and of the fully localized electron for which $\tau_W = \infty$. Long τ_W values, typically for interactions involving *d*-levels, also gives rise to an excess DOS near the resonance energy. The corresponding intuitive picture is that in the mixed $|\Psi>$ state, the electron spends an amount τ_W of its time on the impurity, where it doesn't conduct, and the remainder of its time in the extended states, where it does. In this picture, conduction of heat and charge occurs through RL's even when the impurities are very dilute (ppm levels) and there is no overlap between the wavefunctions of the $|\Psi>$ states. When the impurities are more concentrated (perhaps on the order of a few %), the picture changes: now an overlap exists between neighboring $|\Psi>$ states so that the RL's can form an impurity band that conducts.

This journal is © The Royal Society of Chemistry 2012

Up to now, we only considered an empty band. Since thermoelectric materials must be doped, it is clear that the location of the Fermi level E_F vis-à-vis E_D must matter as well. The following discussion summarizes the physical concepts necessary to exploit resonant levels (RL's) in thermoelectric semiconductors: five criteria need to be met.

1) For zT to be optimal, it is necessary to design a semiconductor with the correct carrier density that optimizes the power factor. Therefore the Fermi level E_F must be located at the correct value.

2) The condition that we need to have the Fermi level close to the central energy E_D of the RL in order for it to modify transport imposes a condition on the position of E_D vis-à-vis the band edge of the host material.

3) Mahan and Sofo[6] calculate that the narrower Γ, the higher the zT (with the limitations due to the background DOS explained in section (1)). In practice, experimentalists have only a certain degree of control over the sample chemistry and defect chemistry and thus over E_F: they need a sufficient width, $\Gamma \sim 10$–100 meV, to be able to locate E_F inside the RL.

4) The RL must conduct charge and heat. In the picture above, this imposes a requirement on the Wigner delay time[30] of the interaction between electrons of the host and the RL, which can be met only through the choice of the guest specie and more particularly of the orbital quantum number of the electronic level of that guest specie that gives rise to the resonance.

5) Mahan and Sofo[6] also show that the background DOS must be as small as possible.

Criteria (3) and (4) above are related as follows. The width Γ of the RL is quite different in metals from what it is in semiconductors, because of the factor $g(E)$ in the expression for Γ in eqn (4). In metals, the background $g(E)$ is filled up to E_F; it is very large and accommodates on the order of one or a few electrons per atom. Consequently, in order to have a Γ sufficiently narrow to have a measurable effect on transport properties, the value of the matrix element $|<O|V|\mathbf{k}>|^2$ must be small, and indeed RL's are observed for *d*-electrons; *s* or p electrons would result in RL's that are much too broad to be noticed. In contrast, in semiconductors, $g(E)$ integrated up to E_F accommodates only 10^{-4} to 10^{-2} electrons per atom: using *d*-levels will now result in impractically narrow Γ values. Simultaneously, the Wigner delay times for *d*-levels are long, which decreases the conductivity of those states. In metals, where the background conductivity is overwhelming, RL's contribute mostly by scattering the host electrons resonantly, a phenomenon we will describe in the following paragraph. In semiconductors, one can hope to see their contribution not only through scattering, but by their own intrinsic contribution to conduction. In practice, we observe that indeed optimal RL's for thermoelectric applications involve *s* and *p* levels, such as those of the group III elements in PbTe or Sn in Bi_2Te_3.

Electronic band structure calculations (see section 5) can identify the nature of the RL and of the interactions that give rise to them, but at the present time they are not precise enough to predict the energy values of E_D, E_F and Γ with the accuracy necessary to optimize thermoelectric performance, nor the degree of localization of the states. This situation is complicated by the temperature dependence of the entire picture, which is crucial for thermoelectric applications.

Of particular interest are RL's in narrow-gap semiconductors. L. A. Fal'kovskii[31] pointed out, on a theoretical basis, that resonant levels are likely to exist in very narrow-gap semiconductors, particularly those with a strongly non-parabolic dispersion relation. The rudimentary and obvious argument is that the narrower the gap, the higher the probability that an impurity level will coincide with a band. The real argument is more subtle: electrons in very narrow-gap semiconductors and semimetals typically have very small effective masses, and thus long de Broglie wavelengths compared to the interatomic distances. The longer the de Broglie wavelength of the electrons in the bands of the host solid, the more they hybridize with the wavefunctions of extra electrons on impurities, and the more likely we are to find RL's that behave more like extended states.

One last concept that will be mentioned here is that of *Fermi level pinning*: when a doping impurity has an E_D in the band, but has a mixed $|\Psi>$ state that is more localized, electrons in that state do not contribute to the Hall effect measurements that are used to measure the free carrier concentration n. The result is then that the relation between n and the concentration of the impurity atoms saturates, and the Fermi energy E_F in essence becomes pinned to E_D. Since in this case, the charge carriers do also not contribute to electrical conduction or thermopower, the observation of Fermi level pinning is not usually conducive to improve the thermopower. A more detailed discussion of impurity band conduction and Fermi level pinning will follow in the section 5 where we will contrast the cases of thallium and titanium resonant impurities in PbTe.

3. Thermopower enhancements

3.1 Theory

The influence of resonant levels on the thermoelectric transport properties arises from two effects:

(i) the excess density of states (DOS) itself at the energy corresponding to the resonant level, and

(ii) the fact that the resonant state diffuses conduction electrons in a way that is extremely sensitive to their energy, and effect known as "resonant scattering".

The first effect is a band structure property that is no more temperature-dependent than the band structure itself, with a minor effect due to temperature-dependence of the chemical potential as a result of T-dependence on the Fermi–Dirac (F-D) distribution. Therefore it becomes the dominant mechanism increasing the thermopower at and above room temperature. The second effect was first identified in metals[32] where the effect of the DOS is negligible because the resonant levels create only a very small excess DOS compared to the large background DOS of the extended states. Resonant scattering theory was later applied to semiconductors,[26] and has been reviewed by Ravich.[33] In this section, we offer first a simple phenomenological theory for both effects, and then suggest that magnetic fields can be used to separate their influences experimentally.

The phenomenological model is based on the Mott equation[34] that relates the thermopower S to the energy-dependent "Mott" conductivity $\sigma_E(E)$. In crystalline solids, both the energy-dependent "Mott"-conductivity $\overleftrightarrow{\sigma}_E(E)$ and the total electrical conductivity $\overleftrightarrow{\sigma}$ are tensors; defining each component (μ,ν) of the

conductivity tensor as $\sigma_{\mu,\nu}$, that component is related to the same component of the "Mott" conductivity by:

$$\sigma_{\mu,\nu} = \int_0^\infty \sigma_{E,\mu,\nu}(E)\left(-\frac{\partial f}{\partial E}\right)dE \tag{5}$$

where f is the F-D distribution function and $E = 0$ is defined at the band edge. The general form for the Mott relation is

$$S = \frac{k_B}{q}\frac{1}{\sigma_{\mu,\nu}}\int_0^\infty \sigma_{E,\mu,\nu}(E)\left(\frac{E-E_F}{k_BT}\right)\left(-\frac{\partial f}{\partial E}\right)dE \tag{6}$$

which we represent as a scalar, thereby assuming that the Fermi surfaces maintain their shape as the energy is changed. Such a result is consistent with the fact that the thermopower is closely related to the entropy of the electron divided by its charge, although that concept is strictly only applicable in reversible thermodynamics (excluding heat transport). Eqn (6) is only applicable to a solid in which the Fermi surface consists of a single pocket (the "single-band case"); a more general tensorial formulation of eqn (6) can be written to describe the thermopower of solids in which the Fermi surface contains more than one pocket. Indeed, the overall thermopower of an anisotropic solid with several pockets in its Fermi surface is a tensor, because it is the average of the partial thermopowers of each pocket weighted by the partial conductivities, which are tensors. A Bethe-Sommerfeld expansion of eqn (6) valid for degenerate statistics and the single-band case yields an approximate formula:[35]

$$\begin{aligned} S &= \frac{\pi^2}{3}\frac{k_B}{q}(k_BT)\left[\frac{1}{n(E)}\frac{dn(E)}{dE}+\frac{1}{\mu(E)}\frac{d\mu(E)}{dE}\right] \\ &= \frac{\pi^2}{3}\frac{k_B}{q}(k_BT)\left[\frac{g(E)}{n(E)}+\frac{1}{\mu E}\frac{d\mu(E)}{dE}\right] \end{aligned} \tag{7}$$

where μ is the mobility (or mobility tensor element $\mu_{\mu,\nu}$). This yields acceptable results in circumstances of practical importance: for PbTe or Bi_2Te_3 doped to about 10^{19}cm^{-3} carriers and temperatures at or below 700 K, its accuracy is only about 30%;[36] an improved Bethe-Sommerfeld expansion that includes second-order corrections and a low-energy cutoff at the band edge (neglected in (5-7)) is[36]:

$$S = \frac{k_B}{q}\frac{\frac{\pi^2}{3}\left(\frac{\sigma'}{\sigma}k_BT\right)\left\{1-\frac{1}{4}\left[2\frac{E_F}{k_BT}+\left(\frac{E_F}{k_BT}\right)^2\right]\exp\left(-\frac{E_F}{k_BT}\right)\right\}+(\ln 2)\left(2+\frac{E_F}{k_BT}\right)\exp\left(-\frac{E_F}{k_BT}\right)}{1+\left(\frac{\sigma'}{\sigma}k_BT\right)(\ln 2)\left(2+\frac{E_F}{k_BT}\right)\exp\left(-\frac{E_F}{k_BT}\right)} \tag{8a}$$

where

$$\frac{\sigma'}{\sigma} = \frac{g(E)}{n(E)}+\frac{1}{\mu(E)}\frac{d\mu(E)}{dE} \tag{8b}$$

Eqn (7) or (8) can be viewed as consisting of two terms that correspond exactly to those outlined in the beginning of this paragraph:

(i) $g(E)/n(E)$, which is the density-of-states (DOS) term

(ii) $(1/\mu)(d\mu/dE)$, which is the scattering term.

The presence of resonant levels will affect both terms of eqn (7) or (8). The contribution of a hump in the DOS as shown in Fig. 1(b) on (i) is obvious, and remains in effect as long as the RL modifies the original band structure rather than develop a separate band. The contribution of that hump on (ii) is known as *resonant scattering*, and requires a longer explanation that is given below. When resonant impurities are added to a solid, the band structure deviates from that of the host solid. If the distortion is relatively slight, as it is in the case of metals, g/n in eqn (7) is small, and the resonant impurities act mostly through the $1/\mu(d\mu/dE)$ term and resonant scattering. In semiconductors like Tl:PbTe[24] and Bi_2Te_3:Sn,[25] the g/n term is important because the background density of states and its integral over energy, $n(E)$, is much smaller than in metals.

The energy dependent relaxation time in the presence of resonant scattering was described by Ravich[33] with a formula inspired from the Lorentzian broadening of the RL (4):

$$\tau_r(E) = \tau_0\left(1+\left(\frac{E-E_D}{\Gamma/2}\right)^2\right) \tag{9}$$

where Γ is the resonant level width, E_D is the resonant impurity band center and τ_0 is the minimum value of $\tau_r(E)$ reached at E_D. Background electron scattering mechanisms, such as acoustic phonon scattering, remain in effect: assign them a relaxation time τ_a. Assuming that resonant scattering works independently from these background mechanisms, the total relaxation time can be obtained from adding the scattering frequencies (Matthiesen's rule):

$$\frac{1}{\tau(E)} = \frac{1}{\tau_r(E)}+\frac{1}{\tau_a(E)} \tag{10}$$

If the strongly energy-dependent behavior of eqn (9) carries through eqn (10), *i.e.* if phonon scattering is not dominant, this provides an effective energy-filtering mechanism that affects the thermopower; hence the label "resonant scattering". However, at high temperatures where $\tau_a < \tau_r$ the effect of resonant scattering disappears.

A didactic qualitative example of the relative effects of the two terms on S in a semiconductor is presented next and in Fig. 4. For clarity, both terms in (8) are treated separately in the top panels, although both of course work simultaneously, and the resulting thermopowers are compared in the bottom panel. In this example, which is based on PbTe, the Kane band model[37] with a DOS-effective mass $m^* = 0.17\ m_e$ and a band gap $E_g = 0.32$ eV is used for the host semiconductor. DOS values $g(E)$ are derived from the mass and converted in units of states/eV/primitive cell using the PbTe lattice constant. Note that we do not model the real case of Tl:PbTe, which is the object of section 5 later, but a model system in which the resonant level is represented by the normalized Lorentz function:

 This journal is © The Royal Society of Chemistry 2012

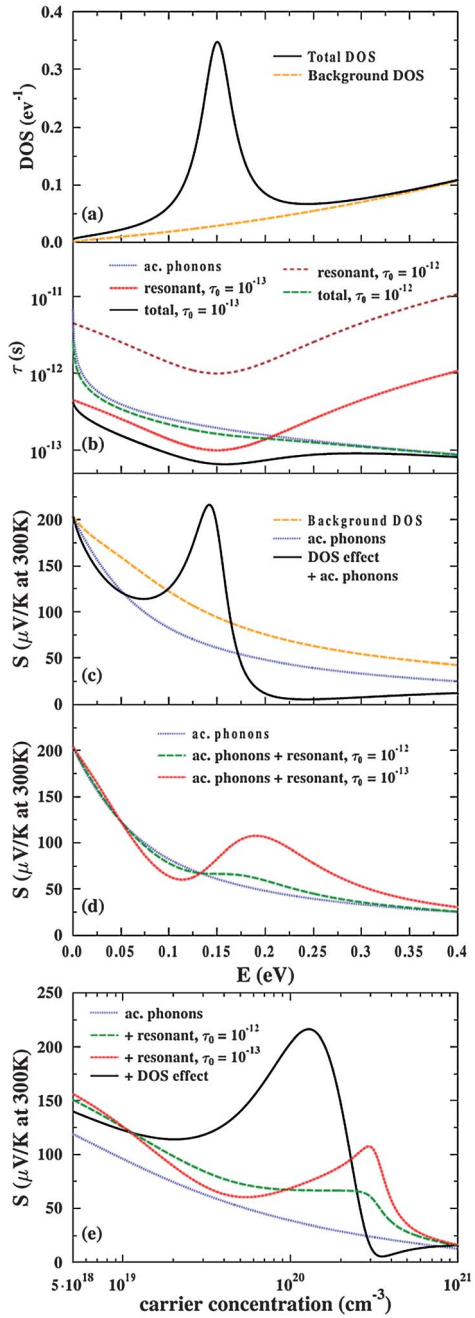

Fig. 4 Schematic representation of the effect of a density of states (DOS) distortion, and of the effect of resonant scattering on the thermopower at 300 K. See text for details. (a) Background DOS (orange) and total DOS after Lorentzian distortion added (black), in following calculations it is assumed that the total DOS comes from a single, distorted band. (b) Relaxation time due to scattering of electrons by acoustic phonons (blue), resonant scattering with $\tau_0 = 10^{-12}$ s (brown) and $\tau_0 = 10^{-13}$ s (red) and total time for those cases, (c) Thermopower at 300 K for the background DOS (orange), background DOS with acoustic phonon scattering (blue) and distorted DOS with acoustic phonon scattering (black). (d) Thermopower at 300 K for the background DOS with acoustic phonon scattering (blue) and its modifications due to resonant scattering with $\tau_0 = 10^{-13}$ s (red) and $\tau_0 = 10^{-12}$ s (green). (e) Comparision of the thermopower at 300 K as a function of carrier concentration for: background DOS with acoustic phonon scattering (blue) and its modifications by resonant scattering or DOS distortion effects. In all cases DOS distortion gives the highest increase in S over the broad energy and carrier concentration range.

$$L(E) = \frac{1}{\pi} \frac{\frac{1}{2}\Gamma}{(E - E_D)^2 + \left(\frac{1}{2}\Gamma\right)^2} \text{ with } \int_{-\infty}^{\infty} L(E) = 1 \qquad (11)$$

centered and maximum at $E_D = 150$ meV, and with a width $\Gamma = 40$ meV. The Lorentz function is multiplied by 0.02, so it can represent a DOS peak accommodating 2 electrons at an impurity concentration of 1%, and this is added to the background DOS, resulting in total DOS shown in Fig. 4(a). The background τ_a is assumed to be acoustic phonon scattering, again with the values corresponding to those in PbTe at 300 K,[38] and an energy dependence $\tau_a \propto E^{-1/2}$. For the resonant scattering term, we use eqn (9) with two realistic values for the parameter τ_0, 10^{-12} and 10^{-13} s. The relaxation time is then calculated from eqn (9) and (10). The thermopower $S(T = 300$ K) shown in Fig. 4(c) and 4(d) is then calculated from eqn (8), with the mobility approximated using an energy-independent effective mass leading to $d\ln(\mu)/dE = d\ln(\tau)/dE$. The thermopower due to the background DOS with acoustic phonon scattering and without it (assuming τ is energy-independent) is contrasted in Fig. 4(c) to the very large effect of the distortion in the DOS due to the resonant level. The distortion in the DOS creates a broad and high maximum in S centered around E_D and with a width of order $\sim$1.5 Γ, that puts S much above the reference value. Fig. 4(d) shows the effect of resonant scattering, illustrating how, when $\tau_a < \tau_r$, the effect of resonant scattering disappears. For the values used in our example, the effect is less pronounced than that of DOS distortion. In the example the maximum in S can be made larger only if unrealistically lower values for the resonant scattering relaxation times are used: for Tl:PbTe at 300 K, values of $\tau_0 < 10^{-14}$ to 10^{-15} s would be needed to reach 150 μV K^{-1}, orders of magnitude lower than the value around 10^{-13} s which is compatible with the mobility observed.[24] Contrasting with the 300 K case discussed here, in the cryogenic temperature range where the phonon relaxation time is much longer, resonant scattering should be observed to increase the thermopower. The DOS effect, being less temperature dependent, enhances S over a broad temperature range.

To summarize, Fig. 4(e) is a calculated Pisarenko plot comparing S as a function of carrier concentration. Here we assumed that the DOS distortion contributes to the carrier concentration even in the case where we calculate the effect of resonant scattering. This comparison shows that the DOS distortion results in a favorable S enhancement over a broad concentration range. For comparison, we show in Fig. 5 the experimental results of the Pisarenko relation for Tl:PbTe published in ref. 24 which are quite similar to even this simple calculation and will be much better modeled in section 5. Indeed, it is worth noting that the different assumed shapes of the RL $g(E)$ peak can lead to different $S(E)$ and $S(n)$ functions. Lorentzian peaks in $g(E)$ give the thermopower maximized over some energy and carrier concentration ranges but broader and less peaked $g(E)$ functions can lead to an enhanced but slowly decreasing $S(n)$ function, as it is presented for the Tl:PbTe case in sections 4.7 and 5.

Obtaining the proper $g(E)$ for the DOS-distortion term (the g/n term in eqn (8)) to enhance S in real semiconductors is subtle: the model above assumed charge carriers to be in a single band. This

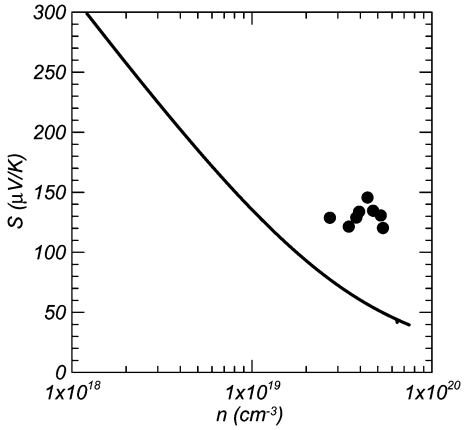

Fig. 5 The Pisarenko relation (thermopower *versus* carrier concentration) between the thermopower S and the hole concentration n in p-type PbTe at 300 K (full line). The points are data for Tl-doped PbTe.

implies that to be effective, the DOS peak must properly hybridize with the background states. Consistently with the discussion in section 2, the DOS peak must originate in extended states that conduct heat and electricity, most likely to be impurity states of *s* or *p*-like character, and not from localized impurity states that often occur when 3*d*-levels of transition metals are involved. The situation is different when the narrow and high DOS peak creates its own narrow impurity band in the same energy range where a background DOS exists. In the absence of hybridization, the thermopower from such a two band system is

$$S = \frac{S_r \sigma_r + S_b \sigma_b}{\sigma_r + \sigma_b} \quad (12)$$

where index the subscript "b" refers to the background band and "r" to the resonant level. Narrow impurity bands are likely to have $\sigma_r \ll \sigma_b$ and the weighted average then gives $S \approx S_b$. The overall conclusion is that an optimal resonant impurity should have as narrow as possible a density of states, (the Mahan and Sofo[6] criterion) but hybridize with the band structure of the host semiconductor. The *s* or *p*-states of impurity atoms are therefore more likely to be most beneficial, even though they are much less likely to create larger DOS distortions than *d*-states. For completion, we wish to remind the reader of the discussion in section 2 on the Wigner delay time. The distinction between localized, "atom-like" states more associated with *d*-states of impurity atoms, and delocalized "plane-wave" like states more associated with *s* or *p*-states, is not black and white but quantitative. Modeling results on Tl:PbTe and Ti:PbTe in section 4.9 will illustrate the point.

The resonant scattering mechanism for enhancing S is not subject to the hybridization condition, since more localized levels still can affect the scattering of background conduction electrons. Indeed, we show in the next section that resonant scattering was observed in 3*d*-elements doped semiconductors like HgSe:Fe.[39] Thermopower enhancements in dilute metallic Kondo systems, such as Au:Fe thermocouple wire, is well established.[12]

3.2 Experimental techniques

Thermomagnetic phenomena are useful to separate experimentally the contributions from band structure effects from those of scattering effects in the thermopower. Two different experimental techniques can be used: low-field transverse Nernst-Ettingshausen measurements, or high-field measurements of the thermopower. The scale of the magnetic field is set by the mobility μ of the sample: a magnetic field is defined as low when the dimensionless product $\mu B < 1$ and high when $\mu B > 1$.

The high-field limit of the thermoelectric power, $S_\infty = \lim_{B\to\infty}[S(B)]$, is independent of the scattering mechanism.[40] Very schematically, since the product of the cyclotron frequency ω_c and the relaxation time τ is also $\omega_c \tau = \mu B$, one can imagine that if this quantity is greater than one ($\omega_c \tau \gg 1$), the carriers move in essence on several cyclotron orbits before they undergo a collision, and their thermopower is almost unaffected by scattering (note that this image cannot be extended to the magnetoresistance, which obviously must remain finite). Therefore, while both scattering and DOS contribute to S at zero field (eqn (7)), the high-field thermopower has only the contribution of the first term g/n, and the effects of the DOS and of resonant scattering can be separated experimentally.

In the low-field limit, and assuming that there is only one type of carrier present in the solid, a technique can be applied that we labeled the "method of the four coefficients".[41,42] In this method, four electronic transport properties are measured on each sample at each temperature–in most cases the thermal conductivity is a fifth transport property measured, but, because it has a phonon contribution, it cannot be used independently here. The four are the electrical resistivity ρ, the thermopower S, the Hall coefficient R_H and the isothermal transverse Nernst-Ettingshausen coefficient N. The latter two properties are measured in low magnetic fields. If the material is isotropic, for instance in crystals with a cubic structure, the measurements can be carried out on either polycrystals or single crystals; if the material is anisotropic, for instance rhombohedral Bi_2Te_3, the measurements are easier to interpret when made along principal axes, such as with the current and voltages in the trigonal plane and the magnetic field along the trigonal axis of Bi_2Te_3. In the method of the four coefficients, it is further assumed that the relaxation time has an energy dependence that is a power law:

$$\tau(E) = \tau_0 E^\lambda \quad (13)$$

where λ, the scattering exponent, is indicative of the dominant mechanism that scatters electrons. For scattering of electrons on acoustic phonons, $\lambda = -1/2$; on grain boundaries or macroscopic uncharged defects, $\lambda = 0$; and on ionized impurities, such as ionized donor or acceptor impurity atoms, $\lambda = 3/2$. If there is only one type of carrier in the solid, either in one single pocket of the Fermi surface, or in several exactly degenerate pockets, then the properties of such electrons are completely determined by four parameters: the electron or hole concentration n, the electron mobility μ, the scattering exponent λ, and either the Fermi energy E_F or the DOS $g(E_F)$ or, if the band is assumed to have a known dispersion relation like a parabola or a Dirac dispersion, the density-of-states effective mass m_{DOS}^*. In such calculation, g and m_{DOS}^* are uniquely related, and n, g and E_F are as well, so they amount to only one unknown. Therefore, at each temperature, one can exactly solve the 4 measured quantities (ρ, S, R_H, N) for the four electronic parameters (n, μ,λ, m_{DOS}^*). If an increase in S related to the presence of an RL is due to the

 This journal is © The Royal Society of Chemistry 2012

DOS effect (g/n in Eqn (17)), this is revealed by an increase in m_{DOS}^* over its value in the host solid; if it is due to resonant scattering ($d\mu/dE$ in eqn (7)), a strong increase in λ is expected.

4. Review of the resonant impurity levels in semiconductors

In principle, resonant levels should exist in all semiconductors; here we review those in bulk III–V, II–VI, IV–VI and V_2-VI_3 compound semiconductors. Many more examples exist of impurity levels that create a DOS peak of mostly localized nature at an energy that coincides with a band of the host material than of those RLs that increase $S(n)$; much recent work seems to indicate that Cd,[43] Sb[44] and Ti[45] belong to the former class in PbTe. For completeness, we mention two special cases first that will not be discussed in detail: size-quantized structures like quantum wells or superlattices, and semimetals.

Size-quantization can affect the existence of RLs, because in a size-quantized structure, the E_D of an impurity does depend on the width of a quantum well or wire. Impurities like Si in GaAs, that are hydrogen-like in bulk material, can become resonant in size-quantized structures.[46] The descriptions that follow in the following paragraphs are strictly limited to bulk semiconductors.

Secondly, the case of semimetals is rather special. At first sight, all electrically active dopants should be resonant impurities in zero-gap semiconductors and in semimetals, since these have a band overlap or a negative band gap. Fal'kovskii's[31] argument (section 2) is also particularly applicable to semimetals like Bi and graphite, in which electrons have extremely small effective masses. Yet no RLs have been identified to date that significantly increase $S(n)$ in the group V semimetals. While a strange temperature-dependence of acceptor doping efficiencies in the semimetal Bi has been observed,[47] to date there is no published in-depth and systematic experimental study of RL's in semimetals. Semimetals have both electrons and holes, whose partial thermopowers are of opposite sign and counteract each-other, making them poor thermoelectric materials. It is, however, conceivable that if RL's were discovered in semimetals like Bi or Sb, they could dominate conduction sufficiently to overcome this fundamental limitation.

4.1 III–V compounds

Reviews of calculations of impurity levels in III–V compounds have been published by Bassani *et al.*[48] and by Iadonisi and Zuchelli.[49] The chalcogens S, Se, and Te are mentioned as potential resonant donors in the heavy III–V compounds InAs and InSb. Experimentally, Se has been observed to give an energy level inside the conduction band of GaSb.[50,51] The conduction band of GaSb consists of a minimum at the Γ-point of the Brillouin zone, with a second minimum at the L-points (like the minima in Ge or PbTe) about 150 meV higher than the Γ - point minimum at 77 K (see Fig. 6). It gives a hydrogen-like level with respect to the L-point minima with a binding energy $R^* \sim 80$ meV below the L-point minimum. This puts the Se level about 70 meV above the Γ - point minimum, and so there is no real ionization energy since the electron can escape the Se level and reach the Γ - point minimum with just a phonon to satisfy the momentum conservation condition. Physically, in the vicinity of the Se atom, two non-degenerate orbital ground states are available to the "extra" non-bonding electron. However, the effective mass of the delocalized electrons at the Γ - point minimum is very small ($m^* \sim 0.04\ m_e$), which results in a large Bohr radius and de Broglie wavelength. The wavefunctions of the neighboring Se impurities will overlap with those of the electrons at the Γ - point minimum, and Se forms a resonant level. This is much less the case with respect to the high-mass ($m_{DOS}^* \sim 0.7\ m_e$) electrons in the extended states at L-point, where the picture is more "atom-like". This illustrates Fal'kovskii's[31] argument in GaSb, but with the difference that here a (presumably phonon-mediated) transfer of momentum from the Γ - point to the L-point is necessary.

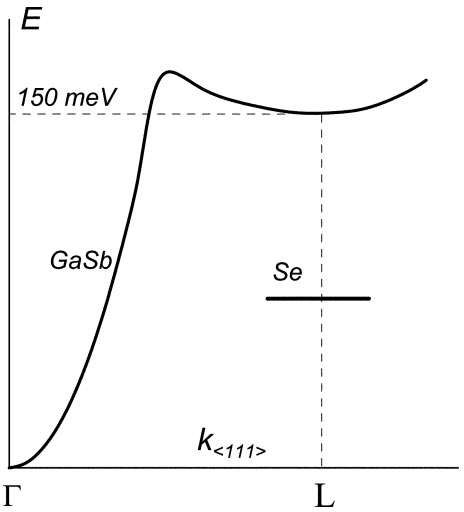

Fig. 6 Schematic dispersion relation for GaSb at 77 K, showing the position of the energy level of Se donors.

Interesting possibilities concern isoelectronic impurities in III–V compounds. A resonant state has been identified in GaAs with Al as an impurity using Hall effect. This state lies 205meV above the Γ edge in at x = 0.29. For $x > 0.29$, the same state appears in the band gap as a deep level and a reduction of the mobility is observed due to resonant scattering.[52] On the pnictide site, Sb in GaAs[53] might act as a resonant impurity. To the knowledge of the authors, no enhancement of the thermopower over the Pisarenko relation has yet been reported in III–V semiconductors.

4.2 II–VI compounds

Tsidil'kovskiĭ[54] reviewed the resonant donor states induced by transition metal elements in II–VI compounds from ZnS to HgTe. Particularly interesting are the zero-gap compounds, like $Hg_{1-x}Cd_xSe$ for x = 0.14, because they correspond to Falkovskii's[31]calculations. A schematic summary[55] of the position of the energy levels of transition metals Sc through Ni, and Cu, in charged states +1 and +2 with respect to the conduction and valence band edges of several II–VI compounds is shown in Fig. 7, which illustrates that many impurities fall in the bands. The transition metals are on the Zn, Cd or Hg site. The energies in the ordinate axis have been adjusted so that the conduction band edge roughly corresponds to the calculated electron

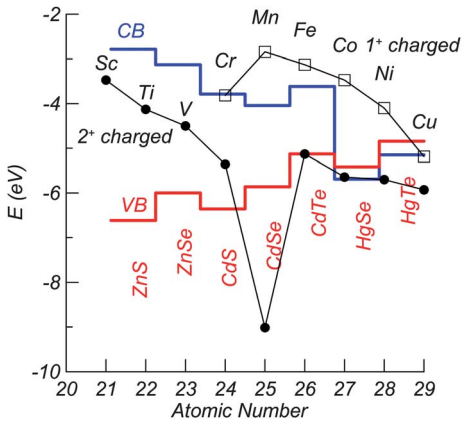

Fig. 7 Energy levels of transition metal impurities (atomic number is the abscissa axis) as donors in their 2^+ charged state, and as acceptors in their 1^+ charge stated, with respect to the conduction and valence band edges of several II–VI compound semiconductors (adapted from ref. 55). The abscissa has no significance for the semiconductors.

affinity[56] (±0.2 eV), but the latter depend on the presence of surface charges.

Impurities displaying *Fermi-level pinning effects* are Fe and Cr in HgSe, although the data for Cr are less elegant than for Fe.[54] The main observation in the Fe in HgSe system is that the concentration of free electrons, n, increases with increasing the iron concentration N_{Fe}, until $n \sim 4.5 \times 10^{18}\text{cm}^{-3}$; above that concentration labeled $N_{Fe}{}^{CRIT}$, adding Fe has no effect. The model is that Fe forms a resonant level about 210 meV above the conduction band edge (a similar model will be illustrated graphically for Ti:PbTe in Fig. 8, section 4.3). Since Fe substitutes for Hg, its "neutral" valence is Fe^{2+}, Fe^{3+} acts as a donor. For $N_{Fe} < N_{Fe}{}^{CRIT}$, iron goes in as $Fe^{3+} + 1e^-$. When $N_{Fe} > N_{Fe}{}^{CRIT}$, any N_{Fe} in excess of $N_{Fe}{}^{CRIT}$ goes in as Fe^{2+}. The values for the respective critical charge carrier concentrations seem to be $N_{Fe}{}^{CRIT} \approx 5 \times 10^{18}\text{cm}^{-3}$ for iron and $N_{Cr}{}^{CRIT} \approx 3 \times 10^{18}\text{cm}^{-3}$ for chromium. It is interesting to follow the Fe resonant level in the $Hg_{1-x}Cd_xSe$ system, in which the conduction and light valence bands close as a function of increasing x, to reach zero for x = 0.14, and then open up again for x > 0.14. It appears that the Fe level is pinned at a constant energy above the level of the heavy valence band. The thermopower of HgSe:Fe shows a strong enhancement at T < 10 K, compared to similar Co-doped samples.[57] This might be attributable to resonant scattering, but the data are new and the proof is not yet conclusive. Dietl[58] has also pointed out the possibility that strong electron-electron interactions may open a gap in this system.

4.3 Rocksalt IV–VI compounds

Alloys of the group IV–VI compound are semiconductors and crystallize in the rocksalt structure. They are the mainstay of thermoelectric technology aimed at operating near 500 °C, where combustion processes typically provide the heat. The binary semiconductors in this class are PbTe, PbSe, PbS, SnTe and GeTe in its high temperature phase. High zT materials based on them are PbTe[59](both p-type[60] and n-type[61]), $PbTe_{1-x}Se_x$,[62] $PbTe_{1-x}S_x$,[63] $Pb_{1-x}Sn_xTe$,[64] $Pb_{1-x}Sn_xTe$-PbS,[63] PbTe + $AgSbTe_2$ (LAST),[65] SnTe + $AgSbTe_2$[66] and GeTe + $AgSbTe_2$ (TAGS).[67] Divalent metal M^{2+} substitutions (M ≠ group IV element) on the Pb site in $Pb_{1-x}M_xTe$ and $Pb_{1-x}M_xSe$ alloys were studied with M = Eu,[68] Ba[69] and Sr.[69,70] Here the substitutions result in large increases of the energy gap of the material, but not in charge transfers, so that Eu and Sr cannot be labeled as dopants. $Pb_{1-x}Sr_xTe$ has recently been revealed to be a very good n-type thermoelectric alloy.[71] Sm is also reported to behave as a divalent impurity in monotellurides.[72] $Pb_{1-x}Mn_xTe$,[73] Ge_{1-x} Mn_xTe,[74] $Pb_{1-x}Mn_xSe$[75] and quaternary IV_{1-x}-Mn_x-VI alloys all exist. Mn being mostly divalent, it is supposed to be electrically inactive–early reports exist that it acts as a donor. The Mn alloys have been extensively studied for their magnetic properties, and discussing them falls outside the scope of this review. Dopants of IV–VI compounds, *i.e.* atoms that transfer charge to the semiconductor lattice, fall in five main classes:

(a) *Off-stoichiometric compositions*: an excess of chalcogen creates vacancies on the metal site and dopes the material p-type. Some of the IV–VI compounds can also be doped n-type with an excess of metal while others, like SnTe, cannot due to the fact that Sn vacancies dominate the defect chemistry.

(b) *Classical extrinsic donor and acceptor impurities*: Classical donor impurities are halogen atoms (Cl, Br and I) substituting for the chalcogens without producing any resonant levels. Classical acceptor impurities are the alkali (Li, Na) atoms substituted for the group IV metals; none are reported to be resonant levels either. The behavior of pnictogens in IV–VI compounds is more differentiated. Bi on the group IV site is a simple donor. Sb is amphoteric in PbTe:[44] when on the Pb site it is a simple donor, but it can be forced to go on the Te site, where it becomes an acceptor. This was theoretically suggested to be a resonant level, but experimentally no increase in thermopower was observed.[44]

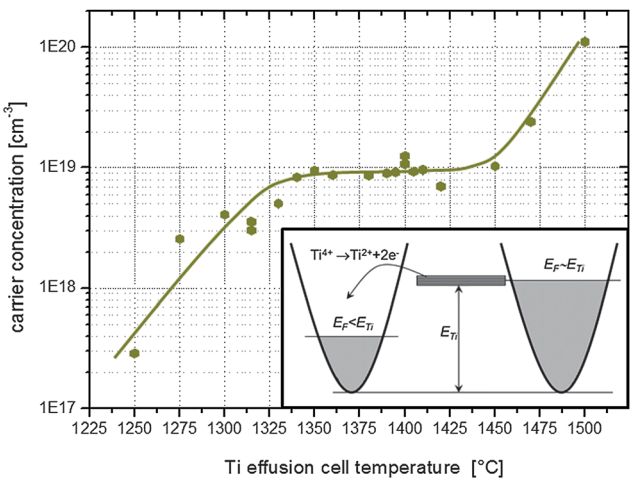

Fig. 8 Illustration of Fermi level pinning in Ti:PbTe. The figure shows the electron concentration at 300 K as measured by Hall effect, plotted as a function of the Ti-cell temperature. Since the vapor pressure of Ti is an exponential function of the cell temperature, the abscissa axis is equivalent to the logarithm of N_{Ti} (the density of Ti atoms in the film). The electron concentration rises proportionally to N_{Ti} until it reaches 1×10^{19} cm^{-3}, after which it remains constant. The insert shows the band structure model, depicting the donor state as being Ti^{4+}, although it is not known yet if it is Ti^{4+} or Ti^{3+}. (Reprinted figure with permission from ref. 45, © 2011 by the American Physical Society).

This journal is © The Royal Society of Chemistry 2012

(c) *Dopants and dilute alloys with transition metals*: in PbTe, Cr, Fe, Co, Ni, Ti, and Ta are reported to be donors.[37] Titanium is a resonant donor[45] with a level in the conduction band. It does give rise to the Fermi level pinning effect,[45] as is illustrated for samples grown by molecular beam epitaxy (MBE) in Fig. 8, which shows the carrier concentration as a function of oven cell temperature. Because the vapor pressure in the Ti flux, and thus the incorporation rate of Ti in the film, varies exponentially with cell temperature, Fig. 8 is equivalent to a log-log plot of *n versus* N_{Ti}. The electron concentration measured by Hall effect, *n*, is proportional to N_{Ti} up to a critical value N_{Ti}^{CRIT}, as was the case for Fe in HgSe, which corresponds to $n \approx 1 \times 10^{19}$ cm^{-3}. A schematic diagram is inserted in Fig. 8: as long as $E_F < E_{D,\,Ti}$, Ti substitutes for Pb as either Ti^{3+} or Ti^{4+} and acts as a donor. Any additional Ti atoms substitute for Pb as Ti^{2+} and are inactive, thus pinning the Fermi level. The increase in *n* as the cell temperature exceeds 1450 °C is attributed to the formation of an impurity band. In the constant-*n* regime of Fig. 8, the electrons in the RL level are expected to be localized and do not contribute to the Hall effect. Ipso facto, they also do not contribute to the thermopower and no increase in thermopower over the Pisarenko plot is observed.[45,76] Preliminary calculations on Ti:PbTe are reviewed in section 5.

Iron is also a donor, and has the interesting property of resonantly scattering phonons.[77] Cr in PbTe appears to be in a Cr^{2+}/Cr^{3+} charged state,[78] where the trivalent state acts as a donor and might display Fermi level pinning. No investigation of the thermoelectric properties of Cr-doped PbTe is yet published, because this is not a promising system as the Cr level is known to move out of the conduction band and into the gap as the temperature is increased just about 300 K.[79] Ravich[37] reports Zn and interstitial Cu to be donors. Cd was expected to have an excess DOS that could result in a large thermopower,[80] but again no enhancement in thermopower was observed.[43] Ag is amphoteric in PbTe, acting as an acceptor up to about 10^{19}cm^{-3}, and as a donor above that concentration.[81]

(d) *Rare-earths and actinides*: The properties of dilute alloys of IV–VI compound semiconductors with rare-earth or actinide atoms substituted for the group IV elements are reviewed in section 4.4.

(e) *Group III elements*: they are often deep and resonant levels in the IV–VI compounds, and will be discussed in detail hereunder in sections 4.5–4.8, with band structure model data in section 5.

4.4 Dilute rare-earth and actinide alloys of IV–VI semiconductors

As outlined in the introduction, it is unlikely that the *f*-levels of rare earth and actinide atoms are involved in the transport properties of the IV–VI compounds, yet their influence has been extensively studied and is reviewed here. In general, the rare-earth and actinide atoms that are mostly trivalent are often donors; those that tend to be divalent, like Eu, tend to open the gap.

Most trivalent rare-earth atoms on the Pb site of PbTe act as donors. Lanthanum is a successful but apparently conventional donor in PbTe,[82] where it has been used in high-zT *n*-type PbTe containing Ag_2Te inclusions. There are data on Ho, Dy, Er[83] and Gd;[84] no anomaly in the data which would be indicative of an electrical activity from the 4*f*-levels is observed. Gd was reported to be a resonant acceptor in SnTe, with $Gd^{2+/3+}$ purported to create an energy level about $E_D \sim 200$ meV below the top of the valence band,[85] but because this corresponds to a hole concentration in the mid-10^{20}cm^{-3} it may be of limited use in thermoelectricity. Uranium in $Pb_{1-x}U_xTe$ alloys[86] is a donor.

Divalent Eu is electrically inactive, but opens the gap of all IV–VI compounds in which it has been alloyed. Examples include $Sn_{1-x}Eu_xTe$,[87] $Pb_{1-x}Eu_xTe$[68,88] and $Pb_{1-x}Eu_xSe$, with the selenide case treated in more detail below. The case of Yb in PbTe is more complicated,[89] as it acts partially as a donor but also, like Eu, increases the band gap.

A systematic study of magnetization and transport of dilute $Pb_{1-x}Ce_xSe$, $Pb_{1-x}Pr_xSe$, $Pb_{1-x}Nd_xSe$, $Pb_{1-x}Eu_xSe$, $Pb_{1-x}Gd_xSe$, and $Pb_{1-x}Yb_xSe$ alloys was published by Jovovic *et al.*[90] The Eu-containing sample in that study was the only p-type sample; Ce, Pr, Nd, and Gd are donors, though they display varying doping efficiencies, which is defined as the concentration of extrinsic electrons determined by Hall measurements divided by the concentration of rare-earth atoms per unit volume. We summarize in Fig. 9(a) the doping efficiency of the different rare-earth atoms as they are substituted for Pb.

$Pb_{1-x}Ce_xSe$ displays a non-Curie–Weiss (C-W) behavior, indicating that the Ce^{3+} atoms undergo the effect of a cubic crystal field, with a crystal field splitting energy of 360 K.[91] At higher temperatures a tendency toward a C-W behavior with a strongly antiferromagnetic C-W temperature is reported. Ce acts like an almost-monovalent donor.

$Pb_{1-x}Pr_xSe$ shows a C-W behavior, also with a high antiferromagnetic C-W temperature; the sample was not uniform and the Pr concentration not very reliable; this may account for the

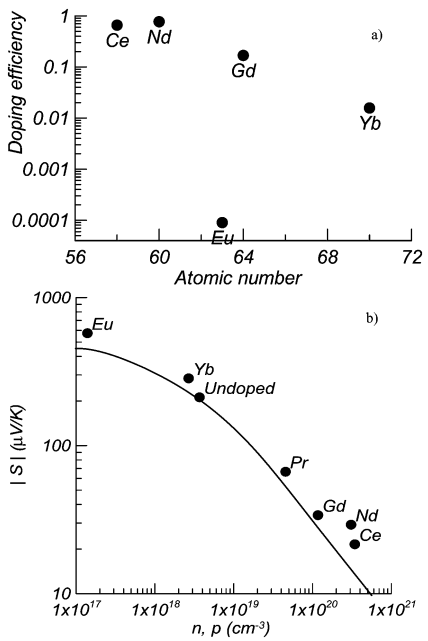

Fig. 9 Rare-earth doping of PbSe: a) doping efficiency *versus* atomic number, b) Pisarenko plot of the thermopower |S| *versus* the log of the carrier concentration n at 300 K. The behavior of Eu stands out: as a divalent atom substituted for Pb^{2+}, it is not a dopant.

low doping efficiency. The reported mobilities may also reflect the presence of a second phase.

$Pb_{1-x}Nd_xSe$ gave pure C-W behavior, and Nd is again a slightly less-than-monovalent donor. The mobility of Nd-doped samples is reduced mostly by ionized impurity scattering, and alloy or magnetic scattering are not needed to interpret the observed values; Nd appears to be an excellent donor for PbSe, much like La is for PbTe.

Eu being divalent, it is not a dopant when substituted to Pb but it opens the gap of $Pb_{1-x}Eu_xSe$ alloys[92,93] following $E_g(x) = E_g$ (PbSe) + 2.16 x ($x < 0.07$). The mobility in $Pb_{1-x}Eu_xSe$ and telluride decreases dramatically with x.[94] $Pb_{1-x}Eu_xSe$ has a pure C-W behavior[90] with a low Curie–Weiss temperature as expected for Eu^{2+} atoms.

$Pb_{1-x}Gd_xSe$ gave pure C-W behavior. Gd is usually found in IV–VI semiconductors in its 3+ charge state. There exists, however, experimental evidence that the $5d^1$ orbital of Gd can be occupied in SnGdTe and PbSnGdTe crystals forming a state resonant with either a valence band (SnGdTe) or a conduction band (PbGdTe).[95] The doping efficiency of Gd is lower than that of Nd or Ce, possibly an indication of the onset of mixed-valence behavior. As with Nd, the mobility reduction is explained by an increased electron concentration.

$Pb_{1-x}Yb_xSe$ has a less clear C-W-like behavior, leading to an uncertain determination of the Yb concentrations in the study,[90] but not so low as to impede the conclusion that the doping efficiency of Yb is much lower than that of Ce or Nd. Adding to that observation the fact that YbSe has a lattice constant that is not aligned with the other trivalent rare-earths, the authors conclude that Yb likely has mixed-valence behavior in $Pb_{1-x}Yb_xSe$. In IV–VI semiconductors Yb is observed in both 3+ ($4f^{13}$, paramagnetic) and 2+ ($4f^{14}$, diamagnetic) configuration with a resonant donor state formed *e.g.* in PbTe and PbGeTe.[96] The mobility is more reduced than expected from ionized impurity scattering alone, perhaps due to the effect of alloy scattering and the presence of electrically neutral Yb^{2+} ions.

Fig. 9(b) shows a Pisarenko plot at 300 K for all samples, most of which (not Eu) are n-type. The full line is calculated with the DOS effective mass of $0.23m_e$[97] for PbSe, and is valid for both CB and VB. The experimental data point for pure p-type PbSe falls on that line; the data points for the rare-earth alloys generally exceed the line, due to a slight increase in effective mass. Interestingly, the data point for $Pb_{1-x}Eu_xSe$ also falls on the line, which suggests that it has a mass similar to that of PbSe, and in strong contrast to the case of $Pb_{1-x}Eu_xTe$ where the mass increases with x: this is discussed in the original paper.[90] $Pb_{1-x}Nd_xSe$ stands out, and has a heavier electron mass than PbSe. With that exception, it appears that the rare-earth donors have little influence on the band structure of PbSe.

4.5 Group III deep impurities in IV–VI semiconductors

Rosenberg and Wald[98] first studied the electrical properties of $Pb_{1-x}In_xTe$ in 1965, and found that In added electrons to the system, but far fewer than 1 electron per impurity atom, which gave the first indications of Fermi level pinning. This was clearly observed in 1971,[99] when the anomalous temperature dependence of the Hall coefficient was also identified. These studies were extended to In-doped $Pb_{1-x}Sn_xTe$.[100] Persistent photoconductivity effects were observed by the Moscow State University group,[101] and the suspicion arose that a cubic-rhombohedral phase transition similar to that in GeTe at 700 K might occur in In-doped PbSnTe at low temperature. Soon thereafter the work was extended to the other group III elements, Tl and Ga. Several of these group III elements were recognized as being resonant impurities, by the observation and calculation of resonant scattering at low temperature.[102] Excellent reviews are given by the Moscow State[27]and St Petersburg[103] groups. It is only recently[24] that it was recognized that not only resonant scattering (the term $d\ln\mu/dE$ in eqn (7)), but also the DOS effect itself (the term g/n in eqn (7)) can contribute to S in these systems, a contribution that persists to room temperature and above. Several specific systems such as Tl:PbTe, $Tl:PbTe_{1-x}S_x$, $Tl:PbTe_{1-x}Se_x$ and $In:Pb_{1-x}Sn_xTe$ will be treated in detail in further sections. In this section, we give a summary of the published experimental data in the binary rocksalt IV–VI compounds, we have the following values for E_D:

a) In PbTe, Tl forms a energy level right at the edge of the upper valence band,[104] though the older literature cites a large variation for the position of this level, and there seems to be a dependence of E_D on Tl concentration, this will be discussed in detail in a separate section. The excess DOS leads to superconductivity and Kondo-like transport properties.[105,106] Indium gives $E_D \sim 90$ meV into the conduction band at $T = 0$ K. Ga appears to display two different levels depending on the Ga concentration and the preparation method.[27] Al is calculated to create an RL near the conduction band edge,[107] but early experimental investigations in the author's group did not find it.

b) In PbSe, Tl displays Fermi level pinning at a hole concentration of $1 \times 10^{20}cm^{-3}$.[108] In early work, In appeared to behave more like a conventional donor in PbSe[98] than in PbTe, but it was later reported that the In level in PbSe may simply lie considerably deeper into the conduction band than in PbTe, with $E_D \sim 300$ meV[109] at 77 K.

c) In PbS and ternary alloys of sulfides and the heavier chalcogens it becomes difficult to follow the Tl level. As the direct L-point gap opens with sulfur concentration, the distance between the light valence band maximum at L-points and the heavy valence band maximum at Σ-points decreases, so that at a certain S concentration, the Tl level becomes degenerate with the heavy valence band. Because the L-point gap is temperature-dependent, the cross-over point also is.

d) In SnTe, In forms a resonant level in the valence band,[110] but the dominance of Sn vacancies in this system, and the fact that they act as acceptors, makes the Fermi level pinning behave almost inversely to what it does in the other RL systems. For each concentration of In in SnTe, there is a range of concentrations of excess Te where the acceptor effect of the Sn vacancy is not observed. As a result, the Fermi level is pinned at the low values of vacancy concentrations, and released above a threshold value, which depends on the In concentration. This is modeled by assuming that E_D is a relatively strong function of In concentration. At low temperature, thermopower enhancements are reported[110] above the calculated Pisarenko relation that holds for the valence band of pure SnTe, and are attributed to resonant scattering.

 This journal is © The Royal Society of Chemistry 2012

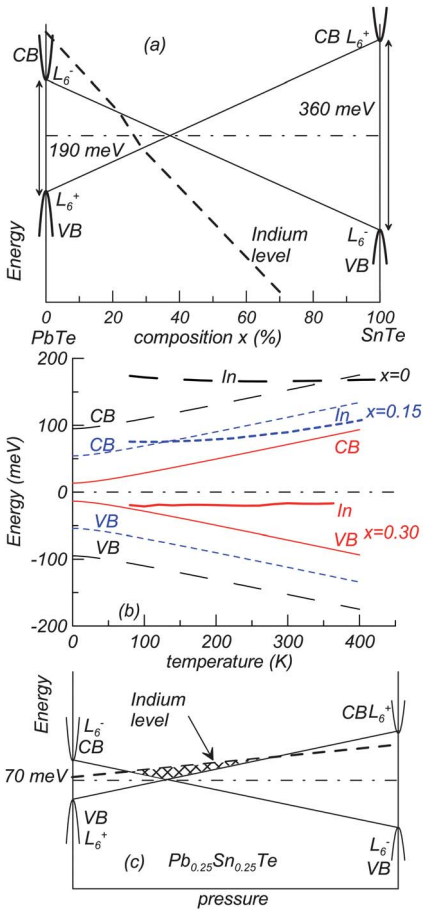

Fig. 10 Composition (a), temperature (b) and pressure (c) dependence of the energy bands (thin lines) and the position of the indium level (heavy lines) in $Pb_{1-x}Sn_xTe$ alloys. In PbTe, the conduction band (CB) is at the L-point of the Brillouin zone, and its symmetry is L_6^-, while the valence band is L_6^+; this inverts in SnTe. The gap of all alloys [in (b), PbTe properties are indicated with long-dashed black lines, $Pb_{0.85}Sn_{0.15}Te$ in short-dashed blue lines and $Pb_{0.7}Sn_{0.3}Te$ in full red lines] increases with temperature, but decreases with hydrostatic pressure. In (c), the In level is resonant only in the hatched pressure region. The abscissa scale is such that the crossing point between the In level and the L_6^- band is ~4.5 kbar, between the In level and the L_6^+ band ~12.5 kbar.

4.6 Indium in $Pb_{1-x}Sn_xTe$ alloys

Both PbTe and SnTe are direct-gap semiconductors that form complete solid solutions, but their conduction and valence bands are inverted[111] (Fig. 10(a)). Consequently, alloys at $x \sim 34 \pm 4\%$ are exactly zero-gap semiconductors at $T = 0$ K, with a pure Dirac dispersion. The energy band structure has very strong temperature dependences (Fig. 10(b)), so that the concentration x at which the gap is zero varies with T. The indium level in $Pb_{1-x}Sn_xTe$ alloys[112] has been studied for a very long time as it is one of the first resonant levels discovered in semiconductors. With increasing x, the In-level moves from the conduction band on the Pb-rich side to the valence band on the Sn-rich side (Fig. 10(a)). The strong temperature dependence of the position of the In level in these alloys has been the object of numerous early partial studies[113,114] and recently summarized by the diagrams shown in Fig. 10(b).[115] In pure PbTe, the In level moves into the energy gap near room temperature, where it acts as a trap, which explains why indium is not a good contact material for n-type PbTe at room temperature. In contrast, the bands of PbTe close under hydrostatic pressure at a rate of $dE_g/dp = 7.4$ meV kbar^{-1}, as shown for one alloy in Fig. 10(c).[116] The indium level is reported to move vis-à-vis the mid-gap point at a rate of $dE_D/dp \sim 1$ meV kbar^{-1}. In a very rough first approximation, all these data indicate that the primary driving force behind the movement of the CB and VB, and of the In-level is the interatomic distance, working either through chemical or mechanical pressure, or thermal expansion. Such a simple description may be attributed to the rather small difference in electro-negativity between Pb and Sn atoms, but the primary role of the interatomic spacing in the physics of RL's will be reinforced by the calculations described in section 5.

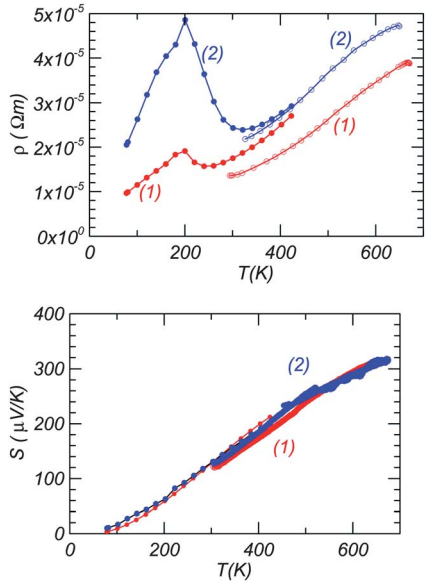

Fig. 11 Top, electrical resistivity ρ and (bottom) thermopower S of two samples of PbTe doped with (1)1at% Tl, and (2) 2 at% Tl. The open and closed dots correspond to measurements made in two different instruments in different temperature ranges (data from ref. 24). The thermal conductivity shows no anomalies and is like that of all binary PbTe with similar resistivity; the zT of the 2% sample is in Fig. 14.

Relevant to the discussion in this review, Jovovic *et al.*[115] show that In does not increase the thermopower of the dilute ($x < 0.3$) PbSnTe alloys. At liquid nitrogen temperatures, however, it was suggested by Hong *et al.*[117] that the low mobilities of n-type In-doped PbSnTe alloys may well be due to a resonant scattering mechanism. However, no anomaly in mobility, thermopower or Nernst coefficient is observed by Jovovic *et al.*[115] who report that the scattering exponent (λ, defined by eqn (13)) remains in the range $-0.2 < \lambda < 0.5$ characteristic of acoustic phonon and ionized impurity scattering.

4.7 Thallium in PbTe, $PbTe_{1-y}Se_y$ and $PbTe_{1-x}S_x$ alloys

While it has long been known that resonant scattering increases the thermoelectric power of Tl:PbTe at low temperature,[27] the effect of the Tl as a RL at room temperature and above is important for applications, because it strongly increases the zT of

the p-type PbTe materials[24] compared to literature values. Fig. 5 shows as data points the thermopower at 300 K of PbTe samples doped with various amounts of Tl, and they are all pinned at about 125–150 μV K^{-1}, considerably above the Pisarenko plot; the temperature dependence of the ρ and S are shown in Fig. 11. Measurements of the transverse Nernst-Ettingshausen coefficient and of the Hall coefficient make it possible to use the method of the four coefficients described above in section 3.3, using those two measurements along that of resistivity and thermopower to determine the hole concentration (3 to 6 × $10^{19}$$cm^{-1}$), mobility (90 to 70 $cm^2V^{-1}s^{-1}$), scattering exponent (eqn (13) becomes $\tau(E) = \tau_0 E^{-1/2}$ indicative of acoustic phonon scattering), and hole density-of-states $g(E)$. The Fermi surface of degenerately-doped p-type PbTe consists of 4 ellipsoidal pockets at the L-points of the Brillouin zone along the |Γ L| direction.[118] The DOS $g(E)$ includes the degeneracy factor of 4, and is further parameterized in terms of a DOS effective mass m^*_{DOS} as shown in Fig. 12, defined as the inverse of the curvature of a parabola drawn through the RL at the Fermi level. For the Tl-doped samples, Fig. 12 shows that the Fermi level is $E_F \sim 60$ meV below the valence band edge; combined with calculations that will be described in section 5 (Fig. 17), that puts the Fermi level firmly in the RL. The DOS effective mass ($m^*_{DOS} \sim 1 \pm 0.3\ m_e$) is roughly 5 times higher than the known mass[118] of the VB of conventionally-doped PbTe at the same hole concentration $m^*_{DOS} \sim$ 0.15 to 0.2 m_e (the latter includes the DOS degeneracy factor of 4, and the effects of non-parabolicity). The value of $m^*_{DOS} \sim 1 \pm$ 0.3 m_e is consistent with the DOS obtained from calculations ($m^*_{DOS} \sim 1.5\ m_e$ is calculated in section 5) and measurements of the electronic specific heat.[119]

That work was extended to $PbTe_{1-x}S$ and $PbTe_{1-y}Se_y$ alloys[104] and the conclusions were reinforced. $Pb_{0.98}Tl_{0.02}Te_{1-x}S_x$ alloys with low sulfur content ($x \leq 0.08$) maintain the excess DOS observed in the binary PbTe doped with thallium; however, the Tl-induced DOS decreases as sulfur content increases to $x = 0.16$. Tl continues to act as a resonant level and results in a thermopower that is pinned at the S at ~120 μV K^{-1} at 300 K for all compositions with $x < 0.08$ (see Fig. 13). Interestingly also, the hole mobility increases with sulfur concentration. Both carrier density and hole effective mass decrease rapidly with y in $PbTe_{1-y}Se_y$, in which the Tl resonant level is partially lost, and

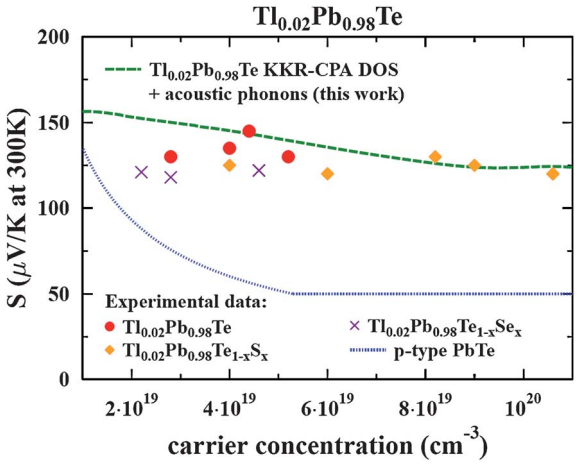

Fig. 13 Thermopower for 2% Tl doped PbTe calculated using KKR-CPA DOS "hump"effect and assuming acoustic phonon scattering (green line). Points correspond to experimental data for Tl:PbTe,[24] $Tl:PbTe_{1-x}S_x$ and $Tl:PbTe_{1-x}Se_x$,[104] and their spread over carrier concentrations is mostly limited by the crystal defect chemistry. Satisfactory agreement between KKR-CPA results and experimental data is obtained.

this was attributed to defect chemistry rather than being an intrinsic band structure property of this system. As in the case of the binary Tl:PbTe, the four-parameter fits in the alloys illustrates that the effect is not due to a change in scattering, but to an increase in DOS; the method determines the experimental DOS-effective mass to be $m^*_{DOS} \approx 1.35 \pm 0.3\ m_e$. Importantly from Fig. 13 it can be concluded that the Tl level in all alloys gives an alloy-independent thermopower, where the band structure is primarily determined by the RL, and the Se or S substitutions for Te only affect the hole concentration. This will be further supported and discussed in section 5. Finally, by using double-doping with both Tl and Na, very high zT values can be obtained from $Pb_{0.98}Tl_{0.02}Te_{1-x}S_x$ alloys (see Fig. 14).

In PbTe and its alloys with S or Se, the enhancement in S, and ultimately of zT, is due to an increase in the local density of states, and not to an increase in the energy dependence of the scattering by resonant scattering. Had the latter been at the origin, one could have expected the effect of the RL to decrease

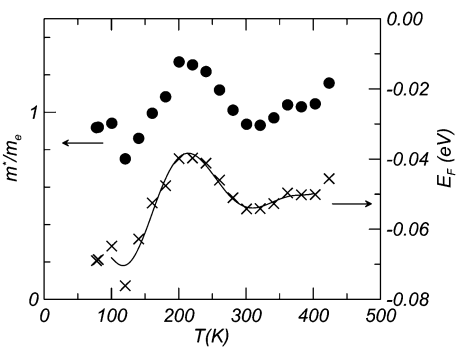

Fig. 12 Temperature-dependence of the Fermi energy E_F and of the density-of-states effective mass (left) of the valence band (dashed line, VB) and of the Tl-doped samples. The mass m_{DOS} is an approximation based on drawing a parabolic band as a dashed line through the RL.

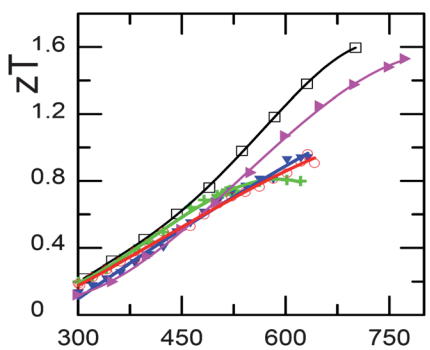

Fig. 14 Thermoelectric figure of merit of $Pb_{0.98}Tl_{0.02}Te$ (purple sideways triangles) after ref. 24, of $Pb_{0.98}Tl_{0.02}Te_{1-x}S_x$ alloys with $x = 0.04$ (blue inverted triangles), 0.08 (open red dots), 0.12 (green+), and of a double-doped $Pb_{0.97}Tl_{0.02}Na_{0.01}Te_{0.92}S_{0.08}$ alloy (black squares). Reproduced by permission of The Royal Society of Chemistry from ref. 104.

This journal is © The Royal Society of Chemistry 2012

with increasing temperature where acoustic and optical phonon scattering become ever more dominating, precluding the use of RL's in high-temperature applications such as electrical power generators.

4.8 V_2-VI_3 compounds

Bi_2Te_3 is the binary semiconductor that is the basis for commercial thermoelectric alloys used for Peltier cooling near room temperature. The upper valence bands (UVB) of degenerately-doped p-type material consist of six ellipsoidal Fermi surfaces in **k**-space,[120] centered along the binary crystallographic direction (along |ΓX|), about 40 ± 10% of the way between the Γ point and the Brillouin zone edge. They have an integral density of states (DOS) effective mass $m^*_{DOS} = 0.35\ m_e$.[120] A lower valence band (LVB), consisting of six ellipsoids, exists 20.5 meV below the UVB in **k**-space along the |ΓA| direction in the bisectrix-trigonal plane (the A-point is the center of the flat hexagonal faces of the Brillouin zone), about 35 ± 5% from the zone center to the zone edge.[120] Bi_2Te_3 can be doped p-type with group IV atoms Ge and Pb. Tin forms an RL with $E_D \sim 15$ meV[121,122] below the top of the UVB at 2 K and "stabilizes" the cryogenic thermopower of single crystals of Bi_2Te_3.[123,124]

Jaworski *et al.*[25] used Sn as a resonant level to strongly increase the thermopower above the Pisarenko relation at 300 K, as shown in Fig. 15. The work was carried out on single crystals in the direction perpendicular to the trigonal axis, but for moderately-heavily doped material, the sample's thermopower is isotropic and equals the scalar partial hole coefficient $S(p)$,[125] which is calculated for p-type Bi_2Te_3 as lines in Fig. 15. The calculation assumed a relaxation time characteristic of two scattering mechanisms, polar optical scattering ($\lambda = 0.5$) and ionized impurity scattering, ($\lambda = 1.5$), and $m^*_{DOS} = 0.35\,m_e$. Fig. 15 shows literature data for Pb and Ge-doped samples[25,126,127] at 300 K. The data measured on the

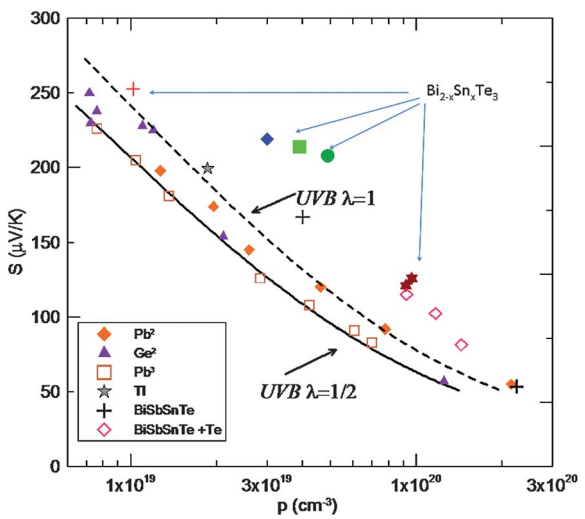

Fig. 15 Pisarenko relation (thermopower *versus* carrier concentration) at 300 K for p-type Bi_2Te_3. The lines are calculated using a classical parabolic band with the effective mass for the UVB. The data points are obtained for the different acceptor impurities as marked. The points where Sn is used as a dopant differ significantly from the others and from the calculated lines.

$Bi_{2-x}Sn_x\ Te_3$ sample depart from the conventional Pisarenko relation, giving strong experimental indication for the presence of an RL. One sample with x = 0.015 has double the S of similarly-doped samples without Sn. The power factors of such samples is also enhanced. Measurements of the period of the Shubnikov-de Haas oscillations on the same samples[25] reinforce the thermopower measurements. Finally, a measurement of the Nernst and Hall coefficients, and the application of the method of the 4 coefficients shows that the effect is partially due to resonant scattering at 100 K, but that it is due to the enhancement of the DOS itself at 300 K. One salient difference between the Sn level in Bi_2Te_3 and the Tl level in PbTe can be seen by comparing Fig. 13 and 14. Where in Tl:PbTe $S(p)$ remains steady at 130–150 μV K^{-1} when increasing Tl atom and hole concentrations, in Sn:Bi_2Te_3 $S(p)$ falls back to the Pisarenko line for $p > 10^{20}$ cm^{-3}. It is possible to over-dope in Bi_2Te_3 with Sn, whereas over-doping does not occur in Tl:PbTe presumably because the solubility limit of Tl is reached before enough Tl can be added to over-dope the samples.

5. Band structure calculations of resonant levels

With the development of powerful methods to calculate the band structure of solids, and the increasing complexity of the formulations of optimized thermoelectric alloys (there are 5 elements in the optimal compound Fig. 14), such calculations are rapidly proving themselves indispensable tools in the quest for resonant impurities capable of enhancing zT. Considering the five criteria that need to be met for this purpose (section 2), modern methods are reasonably accurate at providing some guidance about the value of E_D, but the most difficult property to assess is the degree of localization of the RL state. In this section we will go deeper into the subject, and provide a comparison between a "good" and an "inefficient" RL using as illustrative examples the cases of Tl:PbTe *vs.* Ti:PbTe.

Density Functional Theory[128,129] proved to be very useful and powerful in revealing the physical nature of the impurities in semiconductors, including *e.g.* RL's induced by the group III elements[130] in IV–VI compounds. A systematic *ab initio* study was published for several types of defects in PbTe, such as Pb and Te vacancies, monovalent (Na, K, Rb, Cs, Cu and Ag), divalent (Zn, Cd, Sn, Ge) and trivalent (Ga, In, Tl, As, Sb and Bi) impurities on the Pb site, and Se, S and I sustitutions on the Te site.[80] This was extended to other IV–VI compounds.[131] Of special interest here is a detailed study of the deep levels induced by the group III elements: Tl, In, Ga[132] and more recently Al.[107] The results are shown in the partial charge density maps projected in the <100> plane in Fig. 16. The group III elements (In in this example) substituting for a Pb atom in PbTe (shown as a blue dot in the middle of the frame) form two energy levels. The first, in the left panel, is a hyper-deep defect state (HDS), filled with two electrons per **k**-point. It is predominantly of In-5*s* character; the neighboring states, Te-5*p* states are localized about 0.5 nm from them. The HDS state is full and contains localized electrons. The second level, in the right panel, is called a deep defect state (DDS). It has more contributions of the neighboring Te 5-*p* states, and is only half-filled. The Fermi level is pinned in the middle of this band: as long as the impurity-impurity interactions are weak and no impurity band forms, the position of the Fermi level does not change with impurity concentration. As outlined in

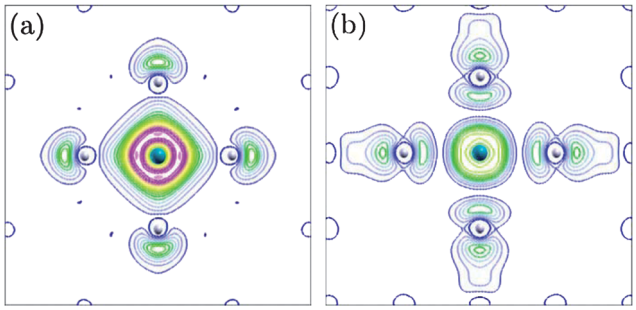

Fig. 16 Partial charge density plot of an In atom on a Pb site in a PbTe lattice, showing the bonding (left, the "hyperdeep" defect state (HDS)) and antibonding (right, the"deep" defect state (DDS)) states of the In-5*s* state and its neighboring Te-5*p* states. The HDS state has a very strong In-5*s* character, is very narrow, and is filled. The DDS state has a mixed In-5*s* and Te-5*p* character, and is less narrow: that state is the resonant level. It is partially filled, which accounts for the Fermi level pinning effects, and is strongly hybridized with the entire valence band. (Reprinted figure with permission from ref. 132, © 2008 by the American Physical Society).

section 4.5, it was suggested from experiment that when the In concentration becomes on the order of 5%, an impurity band forms, and the electrical conductivity becomes dominated by hopping effects.[133]

Aforementioned calculations were done using the super-cell approach, where one builds a large unit cell and replaces one of the host atoms with an impurity atom, creating an ordered structure. Recently a different approach was used to study the effect of a Tl impurity on electronic structure of Pb(Te-Se) and Pb(Te-S) alloys,[104] the KKR-CPA Green function method (Korringa-Kohn-Rostoker with Coherent Potential Approximation).[134] This is computationally advantageous yet reliable in determining electronic structure of disordered systems.[135,136,137] Conceptually, CPA is a mean field theory in which, using the Green function techniques, the real disordered system A_xB_{1-x} is replaced by the ordered system of effective "CPA atoms", described by the effective Green function or alternatively effective scattering operators. The CPA condition means that replacing one of CPA atoms by component A or B atom does not lead to additional scattering and does not change the average properties of the medium. This makes it possible to treat very dilute alloys, with $x \geq 0.1\%$, as all calculations for $0 \leq x \leq 1$ use the same unit cell and the results are not affected by the changes in computational symmetry of the host material.

The DOS of $Tl_{0.001}Pb_{0.999}Te$ is shown in Fig. 17,[138] showing two sharp, core-like DOS peaks arising from the Tl 6*s* states surrounding the main valence band of PbTe. These are the HDS and DDS states.[130,132] Importantly, at this very low concentration, the Tl 6*s* DOS peaks are extremely narrow and large, almost atom-like in nature. In contrast, the Tl 6*p* states are fully integrated into the valence band, which seems to be crucial for Tl bonding in the host compound. Yet, in spite of its narrowness at low Tl concentration, this atom-like resonant level broadens and hybridizes with Te 5*p* states (mostly) when the Tl concentration is increased. This creates a separate 'hump' in DOS (see Fig. 17 for 2%Tl). Its full width at half maximum is now ~200 meV and calculated $E_F = 150$ meV. The observed experimental $E_F \sim 60$ meV may have included the effects of additional doping by the inevitable stoichiometry defects in the crystal.

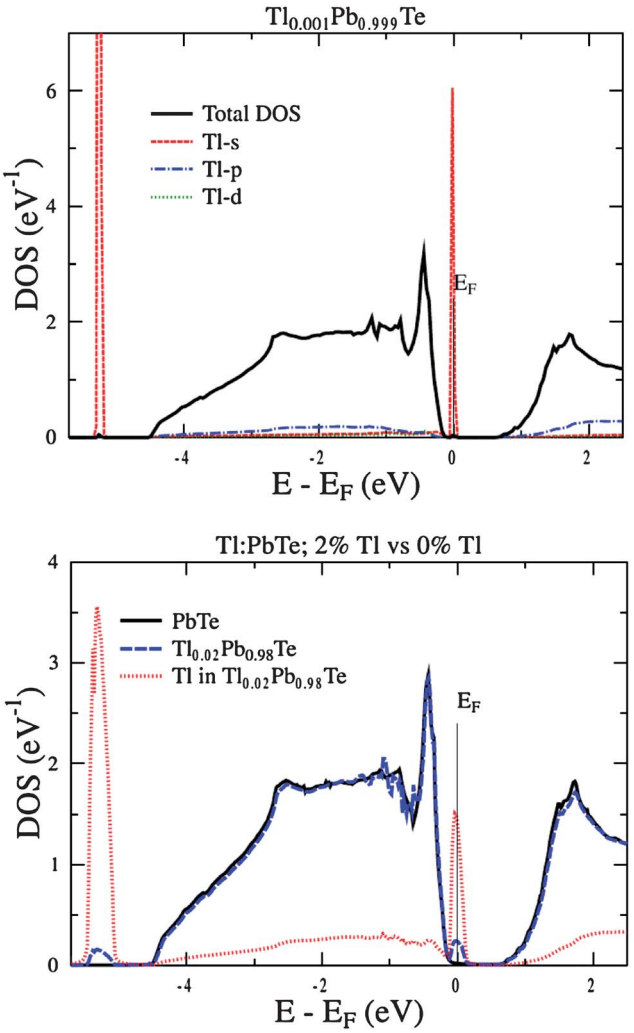

Fig. 17 Calculated density of states for PbTe with Tl impurity, assuming substitutional Tl atom on Pb site with 0.1% concentration (upper panel) and 2% (bottom panel). States located in lower energy range are not shown (6s of Pb and 5s of Te). Upper panel: Black line is a total density of states per formula unit. Partial Tl densities of states (per Tl atom, not multiplied by concentration) are plotted in red (s), blue (p) and green (d). The most striking feature of the electronic structure is the presence of sharp, semi-core-like DOS peaks from 6s states of Tl in the valence band region. Lower panel: For 2% Tl concentration, Tl peak is broadened and hybridization with p orbitals of Te and Pb occurs. This leads to the formation of a DOS 'hump'.

The contributions of the constituent atoms to this hump at E_F are Tl 12%, Pb 15%, and Te 50%, with rest coming from interstitial states. Given the relatively low Tl contribution, it is possible to view the Tl atoms as acting like a catalyst that allows the formation of the excess DOS of PbTe, but Tl itself contributes to it only minimally. The charge located in this new hybridized $s + p$ band comes mainly from Te atoms, and the new states are delocalized and participate in the transport phenomena. The excess DOS between the valence band edge E_V and E_F can be fitted to a $g(E) = a\sqrt{E_V - E} - b$ law, almost like a free electron ($g(E) = a\sqrt{E_V - E}$), with $a = 0.84 \pm 0.02$ $eV^{3/2}$ which in a free electron model would correspond to a mass $m^*_{DOS} \approx 1.5\ m_e$. This calculated value is surprisingly consistent

This journal is © The Royal Society of Chemistry 2012

with the experimental value from the "method of the four coefficients", $m^*_{DOS} \approx 1.35 \pm 0.3\ m_e$ (see section 4.7 and ref. 104). One can conclude that Tl creates resonant-yet-nearly-free-electron-like states in PbTe and its alloys, joining two features that might be perceived as contradictory. On a cautionary note, the presence of constant negative factor $b = 0.1 \pm 0.005$ (eV^{-1}) in the formula above limits the free-electron interpretation and shows the important effects of crystal potentials. Also, since the excess DOS starts right at the VB edge, Fig. 18 shows a schematic dispersion for the Tl RL level in PbTe relative to the upper (UVB) valence band at the L-points of the Brillouin zone, and the lower valence band (LVB) near the Σ-point. This picture updates the one in ref. 24.

From the DOS of Fig. 17, eqn (8), and assuming acoustic phonon scattering, the thermopower of Tl:PbTe can be calculated at 300 K and plotted as a function of calculated carrier concentration. This is done in Fig. 13, where the results are compared to the experimental points. The agreement is remarkable.[139] The free-electron-like DOS in Fig. 17 is less narrow than the Lorentzian in the example Fig. 4, resulting in a less concentration-dependent thermopower; this may have contributed to the agreement. Indeed the experimental values of E_F (60 ± 10 meV) reflects the fact that the carrier concentration is not only a function of Tl concentration, but is also affected by stoichiometry defects in the samples and/or additional Na-doping,[104] while the calculated E_F (150 meV) ignores those facts and rather arbitrarily assumes that each Tl atoms introduces one hole. Independent adjustments of E_F are necessary to maximize zT by fulfilling the conditions outlined by Mahan and Sofo.[6]

The calculations for binary PbTe were extended to its alloys with Se and S:[104] the DOS hump does not change for ~10–15% Te substitution with S, thus the same $S(n)$ curve should apply here. Fig. 13 shows this to be correct up to 10% S substitution; the case of Se substitution was less satisfactory. At larger sulfur concentrations the calculated DOS broadens and merges into the UVB DOS, which is accompanied by a reduction in the excess of $S(n)$ observed in the experiment. The calculations further identify that it is the reduction in lattice constant with the S and Se substitutions that lies at the origin of the merging and smearing of the Tl level. The basic concept is that the reduction in lattice constant increases the overlap between the wavefunctions of the Tl 6*s* and the Te *p*-levels as well as the Pb levels. This results in too strong a hybridization between them, and a merging of the RL into the host solid's DOS.

The case of Ti:PbTe (Fig. 8 and Fig. 19) can be used as a supporting counter-example to Tl:PbTe. It is probably illustrative of the effects of most 3*d* transition-metal impurities in PbTe (section 4.3), although some involve transitions to magnetic states (*e.g.* 1% Cr doped PbTe is a room-temperature ferromagnet[140]) we also limit this discussion to dilute alloys. Fig. 19 shows the results of KKR $2 \times 2 \times 2$ supercell calculations for $Pb_{0.97}Ti_{0.03}Te$: the Ti peak in the DOS is very sharp and narrow. Its contribution to the total DOS at E_F exceeds 50%,

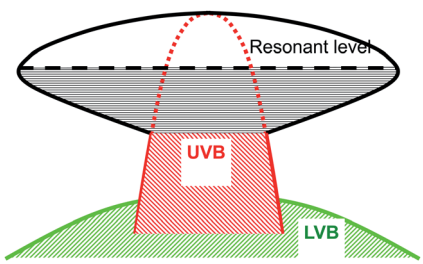

Fig. 18 Cartoon of the valence band structure of Tl-doped PbTe, showing schematically the upper valence band (UVB, red) at the L-points of the Brillouin zone, the lower heavy hole band (LVB, green) which, when populated, forms a crown-like Fermi surface around the Σ-points of the Brillouin zone, and the Tl-induced resonant level (black). The latter has a free-electron-like shape, yet with a heavy density-of-states mass. When the Fermi level is about 60 meV from the valence band edge, the thermopower is pinned to ~120 μV K^{-1} at 300 K. When the Fermi level reaches the LVB, the thermopower at 300 K is only ~50 to 55 μV K^{-1}. Reproduced by permission of The Royal Society of Chemistry from ref. 104.

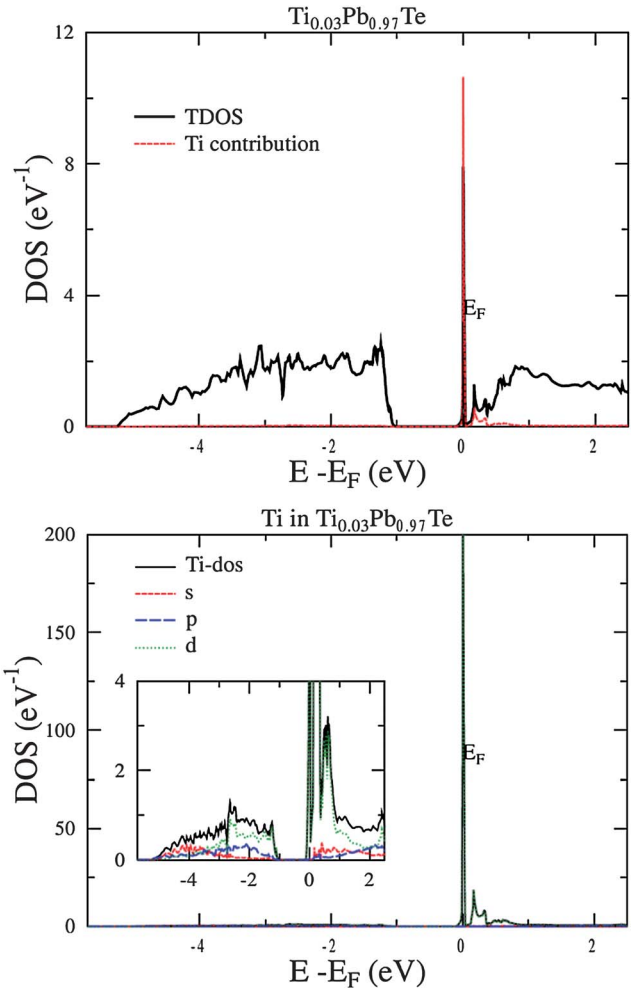

Fig. 19 Calculated density of states for PbTe with Ti impurity, assuming substitutional Ti atom on Pb site with 3% concentration (non-spin-polarized calculations in this work). Upper panel: Total density of states per formula unit plotted in black. The contribution from Ti atoms (here the Ti concentration is taken into account) is plotted in red. Lower panel: partial Ti DOS per Ti atom, with angular momentum decomposition. The sharp and large 3*d* peak suggests the localization of the 3*d* states and a transition to a magnetic state. The t_{2g}-e_g splitting is also visible: the peak comes from E_g states. The inset shows the same plot at a different scale to show *s* and *p* contributions.

and, unlike the case of Tl, it does not "catalyze" a DOS that consists mostly of Te or Pb states. Also, as mentioned in section 2, for *d*-like resonant levels, the Wigner delay time spent by electron at the resonance center becomes long. All this suggests that Ti rather develops its own, mostly localized states in PbTe, which might even create a magnetic instability through the Stoner mechanism.[141] The Ti DOS peak also is placed on top of a large density of PbTe conduction band states, which, following the Mahan-Sofo[6] argument, is also unfavorable to zT.

To summarize, band structure calculations have much to contribute to the understanding of how resonant levels can improve zT. One should look for impurities which create sharp DOS peaks close to the Fermi level, but those peaks should be of the similar character as the host band structure. Consistently with the central role the orbital quantum number of the RL plays in the concept of Wigner delay time, we conclude that *d*- or even *f*-state impurities are useful to improve the thermopower of metals, but that *s*- or *p*-state RL's are more suited to improve thermoelectric properties of semiconductors.

Conclusions

This review focused on the use of resonant impurity levels to maximize the thermoelectric figure of merit zT, by maximizing the thermoelectric power $S(n)$ at a given carrier concentration, which maximizes the power factor $S^2\sigma$. Resonant levels are created by impurities whose electrons have energy levels in a band of the host material. Such energy levels can affect the thermopower through two mechanisms: (1) they can scatter the conduction electrons of the host semiconductor resonantly, which gives these electrons a very energy-dependent mobility; (2) if the energy levels correspond to plane-wave-like wavefunctions that are characteristic of extended states in semiconductors, electrons in them can carry electricity and heat, and contribute to the thermopower. At room temperature and above, mechanism (1) competes with phonon scattering and is often weak; mechanism (2) is a band structure property and more temperature-independent.

The effectiveness of a resonant level in enhancing the thermoelectric power factor by the second mechanism depends critically on the degree of localization of the electrons in the impurity states, itself a function of the amount of hybridization between the impurity states and the band structure of the host semiconductor. As is the case with every other parameter in thermoelectrics research, where a delicate optimization is needed between mutually counter-indicated properties (thermal conductivity *versus* mobility, or thermopower *versus* carrier concentration), the use of resonant levels requires a delicate balancing between two mutually exclusive properties of electronic wavefunctions. Here the counter-indication is between plane-wave-like extended states and atom-like localized. Too much overlap between the impurity and the host material's wavefunctions makes the resulting wavefunctions resemble more those of the host material and decreases the excess in thermopower; too little overlap creates states that could lead to a much larger thermopower, but such states are easily too localized and do not conduct well. To illustrate this point, we contrast the examples of two dopant atoms in a very important thermoelectric semiconductor, PbTe. Thallium creates states at the edge of the valence band, but the impurity only catalyzes the formation of the excess DOS, which is mostly constituted of Te and Pb states; by contrast, Ti forms a state in the conduction band, but it remains over 50% Ti-like, is more 3*d* in character, does not conduct heat or charge, and does not enhance thermoelectric performance. Only resonant states such as those induced by Tl in PbTe are beneficial to thermoelectric applications.

Acknowledgements

This work is supported by the U.S. Air Force Office of Scientific Research MURI "Cryogenic Peltier Cooling", contract FA9550-10-1-0533, and by the U.S. Department of Energy, Energy Frontier Research Center on Revolutionary Materials for Solid State Energy Conversion, 61-3212B.

References

1 A. F. Ioffe, *Physics of Semiconductors*, Academic Press, New York, 1960 (translated from Russian, *Fizika Poluprovodnikov*, Russian Academy of Sciences, Moscow, 1957).
2 We have not been able to find the original reference to N. L. Pisarenko.
3 Christopher J. Vineis, Ali Shakouri, Arun Majumdar and Mercouri G. Kanatzidis, *Adv. Mater.*, 2010, **28**, 3270.
4 G. A. Slack, New Materials and Performance Limits for Thermoelectric Cooling, in *CRC Handbook of Thermoelectrics*, ed. D. M. Rowe, CRC Press LLC, Boca Raton, FL, 1995, p. 407.
5 N. W. Ashcroft and D. N. Mermin, *Solid-State Physics*, Holt, Rhinehart and Winston, New York, 1976.
6 G. D. Mahan and J. O. Sofo, *Proc. Natl. Acad. Sci. U. S. A.*, 1996, **93**, 7436.
7 L. D. Hicks and M. S. Dresselhaus, *Phys. Rev. B: Condens. Matter*, 1993, **47**, 12727; L. D. Hicks and M. S. Dresselhaus, *Phys. Rev. B: Condens. Matter*, 1993, **47**, 16631.
8 J. P. Heremans, *Acta Phys. Polon. A*, 2005, **108**, 609.
9 J. Kondo, *Prog. Theor. Phys.*, 1965, **34**, 372.
10 J. Korringa and A. N. Gerritsen, *Physica*, 1953, **19**, 457.
11 J. Friedel, *Can. J. Phys.*, 1956, **34**, 1190.
12 F. J. Blatt, P. A. Schroeder, C. L. Foiles and D. Greig, *Thermoelectric Power of Metals*, Plenum Press, New York, 1976.
13 M. D. Daybell and W. A. Steyert, *Rev. Mod. Phys.*, 1968, **40**, 380.
14 A. J. Heeger, Localized moments and nonmoments in metals, in *Solid State Physics*, ed. F. Seitz, D. Turnbull and H. Ehrenreich, Academic Press, New York, 1969, vol. 23, p. 284.
15 G. D. Mahan, Good Thermoelectrics, in *Solid State Physics*, ed. H. Ehrenreich and F. Spaepen, Academic Press, New York, 1997, vol. 51, pp. 81–152.
16 Z. Fisk, J. L. Sarrao and J. D. Thompson, *Curr. Opin. Solid State Mater. Sci.*, 1996, **1**, 42.
17 P. Sun, N. Oeschler, S. Johnsen, B. B. Iversen and F. Steglich, *Dalton Trans.*, 2010, **39**, 1012.
18 Hidefumi Takahashi, Yukio Yasui, Ichiro Terasaki and Masatoshi Sato, *J. Phys. Soc. Jpn.*, 2011, **80**, 054708; H. Takahashi, R. Okazaki, Y. Yasui, I. Terasaki, M. Sato, *The 30th International Conference on Thermoelectrics*, Traverse City, Michigan, USA July 17–21, 2011.
19 D. M. Rowe, V. L. Kuznetsov, L. A. Kuznetsova and G. Min, *J. Phys. D: Appl. Phys.*, 2002, **35**, 2183.
20 C. Herring, T. H. Geballe and J. E. Kunzler, *Phys. Rev.*, 1958, **111**, 36.
21 P. E. Nielsen and P. L. Taylor, *Phys. Rev. B: Solid State*, 1974, **10**, 4061.
22 J. B. Goodenough and J.-S. Zhou, *Phys. Rev. B: Condens. Matter*, 1994, **49**, 4251.
23 P. L. Taylor and O. Heihonen, *A Quantum Approach to Condensed Matter Physics*, Cambridge University Press, 2002.
24 J. P. Heremans, V. Jovovic, E. S. Toberer, A. Saramat, K. Kurosaki, A. Charoenphakdee, S. Yamanaka and G. J. Snyder, *Science*, 2008, **321**, 554.

 This journal is © The Royal Society of Chemistry 2012

25 C. M. Jaworski, V. Kulbachinskii and J. P. Heremans, *Phys. Rev. B: Condens. Matter Mater. Phys.*, 2009, **80**, 233201.
26 S. A. Nemov and Yu. I. Ravich, *Phys.-Usp.*, 1998, **41**, 735.
27 B. A. Volkov, L. I. Ryabova and D. R. Khokhlov, *Phys.-Usp.*, 2002, **45**, 819.
28 E. Daniel, J. Friedel, *"Low-Temperature Physics" LT9*, ed. J. G. Daunt *et al.*, Plenum Press, New York, 1965, p. 933.
29 M. H. Cohen, *Can. J. Chem.*, 1977, **55**, 1906.
30 P. Lloyd and P. V. Smith, *Advances in Physics*, Taylor & Francis, 1972, vol. 21, p. 69; B. L. Györffy and G. M. Stocks, in *Electrons in disordered metals and metallic surfaces*, ed. P. Phariseau, B. L. Györffy and L. Scheive. NATO ASI Series, Physics, B42. Plenum Press, NY, 1979
31 L. A. Falkov'skii, *Sov. Phys. JETP*, 1976, **41**, 767.
32 P. de Faget de Casteljau and J. Friedel, *J. Phys. Radium*, 1956, **17**, 27; A. Blandin and J. Friedel, *J. Phys. Radium*, 1959, **20**, 160 (in French).
33 Y. I. Ravich, Selective carrier scattering in thermoelectric materials, in *CRC Handbook of Thermoelectrics*, ed. D. M. Rowe, CRC Press, Boca Raton, FL, 1995, p. 67.
34 N. F. Mott and E. A. Davis, *Electronic conduction in non-crystalline materials*, Clarendon Press, Oxford, 1979.
35 V. Y. Irkhin, Y. P. Irkhin, *Electronic Structure, Correlation Effects and Physical Properties of d- And f-Metals and Their Compounds*, Cambridge Int. Science Publishing, 2007.
36 Y. Gao, G. J. Snyder and J. P. Heremans, *P5, The 30th International Conference on Thermoelectricity*, July 17–21, 2011, Traverse City, Michigan, USA, and manuscript submitted for publication.
37 Yu. I. Ravich, B. A. Efimova and I. A. Smirnov, *Semiconducting Lead chalcogenides*, Plenum Press, New York, 1970.
38 S. Ahmad and S. D. Mahanti, *Phys. Rev. B: Condens. Matter Mater. Phys.*, 2010, **81**, 165203.
39 A. T. Lonchakov, V. I. Okulov, V. L. Konstantinov and K. A. Okulova, *Low Temp. Phys.*, 2009, **35**, 331.
40 W. Zawadzki and R. Lassnig, *Surf. Sci.*, 1984, **142**, 225.
41 J. P. Heremans, C. M. Thrush and D. T. Morelli, *Phys. Rev. B: Condens. Matter Mater. Phys.*, 2004, **70**, 115334.
42 J. P. Heremans, C. M. Thrush and D. T. Morelli, *J. Appl. Phys.*, 2005, **98**, 063703.
43 K. Ahn, M. K. Han, J. He, J. Androulakis, S. Ballikaya, C. Uher, V. P. Dravid and M. G. Kanatzidis, *J. Am. Chem. Soc.*, 2010, **132**, 5227.
44 C. M. Jaworski, J. Tobola, E. M. Levin, K. Schmidt-Rohr and J. P. Heremans, *Phys. Rev. B: Condens. Matter Mater. Phys.*, 2009, **80**, 125208.
45 J. D. König, M. D. Nielsen, Y. Gao, M. Winkler, A. Jacquot, H. Böttner and J. P. Heremans, *Phys. Rev. B*, accepted.
46 T. A. Perry, R. Merlin, B. V. Shanabrook and J. Comas, *Phys. Rev. Lett.*, 1985, **54**, 2623.
47 J. Heremans and O. P. Hansen, *J. Phys. C: Solid State Phys.*, 1983, **16**, 4623.
48 F. Bassani, G. Iadonisis and B. Preziosi, *Rep. Prog. Phys.*, 1974, **37**, 1099.
49 G. Iadonisi and G. P. Zucchelli, *Phys. Status Solidi B*, 1974, **62**, 625.
50 R. T. Bate, *J. Appl. Phys.*, 1962, **33**, 26.
51 K. Hoo and W. M. Becker, *Phys. Rev. B: Solid State*, 1976, **14**, 5372.
52 A. K. Saxena and P. Singh, *Phys. Status Solidi B*, 1996, **195**, 451.
53 V. K. Bashenov, I. Baumann and A. G. Petukhov, *Phys. Status Solidi B*, 1980, **100**, K105.
54 I. M. Tsidil'kovskiĭ, *Sov. Phys. Usp.*, 1992, **35**, 85.
55 D. Heiman, M. Dahl, X. Wang, P. A. Wolff, P. Becla, A. Petrou and A. Mycielski, *Mat. Res. Soc. Symp. Proc.*, 1990, **161**, 479.
56 C. G. Van de Walle and J. Neugebauer, *Nature*, 2003, **423**, 626.
57 A. T. Lonchakov, V. I. Okulov, V. L. Konstantinov, K. A. Okulova and S. Yu. Paranchich, *Low Temp. Phys.*, 2009, **35**, 223.
58 T. Dietl, *Jpn. J. Appl. Phys.*, 1987, **26**(Suppl. 3), 1907.
59 A. F. Ioffe, *Semiconductor Thermoelements and Thermoelectric Cooling*, London, Infosearch, 1957.
60 Y. Pei, A. LaLonde, S. Iwanaga and G. J. Snyder, *Energy Environ. Sci.*, 2011, **4**, 2085.
61 A. D. LaLonde, Y. Pei and G. J. Snyder, *Energy Environ. Sci.*, 2011, **4**, 2090.
62 Y. Pei, X. Shi, A. LaLonde, H. Wang, L. Chen and G. J. Snyder, *Nature*, 2011, **473**, 66.
63 J. Androulakis, C.-H. Lin, H.-J. Kong, C. Uher, C.-I. Wu, T. Hogan, B. A. Cook, T. Caillat, K. M. Paraskevopoulos and M. G. Kanatzidis, *J. Am. Chem. Soc.*, 2007, **129**, 9780.
64 Y. Gelbstein, Z. Dashevsky, Y. George and M. P. Dariel, *Int. Conf. Thermoelectr., 25th*, 2006, 418.
65 K.-F. Hsu, S. Loo, F. Guo, W. Chen, J. S. Dyck, C. Uher, T. Hogan, E. K. Polychroniadis and M. G. Kanatzidis, *Science*, 2004, **303**, 818.
66 Y. Chen, M. D. Nielsen, Y. B. Gao, T. J. Zhu, X. B. Zhao and J. P. Heremans, *Advanced Energy Materials*, 2011, DOI: 10.1002/aenm.201100460.
67 E. Skrabek, D. Trimmer, U.S. Patent 3945855, 1976.
68 G. Braunstein, G. Dresselhaus, J. Heremans and D. L. Partin, *Phys. Rev. B*, 1987, **35**, 1969.
69 D. L. Partin, C. M. Thrush and B. M. Clemens, *J. Vac. Sci. Technol., B*, 1987, **5**, 686.
70 A. Lambrecht, N. Herres, B. Spanger, S. Kuhn, H. Böttner, M. Tacke and J. Evers, *J. Cryst. Growth*, 1991, **108**, 301.
71 K. Biswas, J. He, Q. Zhang, G. Wang, C. Uher, V. P. Dravid and M. G. Kanatzidis, *Nat. Chem.*, 2011, **3**, 160.
72 F. F. Aliev and H. A. Hasanov, *Inorg. Mater.*, 2011, **47**, 853.
73 M. Escorme, A. Mauger, J. L. Tholence and R. Triboulet, *Phys. Rev. B*, 1984, **29**, 6306.
74 R. W. Cochrane, M. Plischke and J.-O. Stoeam-Olsen, *Phys. Rev. B: Solid State*, 1974, **9**, 3013.
75 V. G. Vanyarkho, V. P. Zlomanov, A. V. Novoselava and V. N. Fokin, *Izv. Akad. Nauk SSSR Neorg. Mater.*, 1969, **5**, 1699 (in Russian).
76 M. N. Vinogradova, E. A. Gurieva, V. I. Zharskii, S. V. Zarubo, L. V. Prokof'eva, T. T. Dedegkaev and I. I. Kyukov, *Sov. Phys. Semicond.*, 1978, **12**, 387.
77 D. T. Morelli, J. P. Heremans and C. M. Thrush, *Phys. Rev. B: Condens. Matter*, 2003, **67**, 035206.
78 T. Story, Z. Wilamowski, E. Grodzicka, B. Witkovska and W. Dobrowolski, *Acta Physica Polonica A*, 1993, **84**, 773; E. Grodzicka, W. Dobrowolski, J. Kossut, T. Story and B. Witkovska, *J. Cryst. Growth*, 1994, **138**, 1034.
79 V. D. Vulchev and L. D. Borisova, *Phys. Status Solidi A*, 1987, **99**, K53; V. D. Vulchev, L. D. Borissova and S. K. Dimitrova, *Phys. Status Solidi A*, 1986, **97**, K79.
80 S. Ahmad, S. D. Mahanti, K. Hoang and M. G. Kanatzidis, *Phys. Rev. B: Condens. Matter Mater. Phys.*, 2006, **74**, 155205.
81 D. L. Partin and J. P. Heremans, Growth of Narrow Bandgap Semiconductors, in *Handbook on Semiconductors*, ed. T. S. Moss and S. Mahajan, Elsevier, 1994, vol. 3, pp. 369–450.
82 Y. Pei, J. Lensch-Falk, E. S. Toberer, D. L. Medlin and G. J. Snyder, *Adv. Funct. Mater.*, 2011, **21**, 241.
83 D. L. Partin, *J. Appl. Phys.*, 1985, **57**, 1997.
84 A. Bruno, J. P. Lascaray, M. Averous, G. Filion and J. F. Dumas, *Phys. Rev. B*, 1988, **37**, 1186.
85 T. Story, M. Górska, A. Łusakowski, M. Arciszewska, W. Dobrowolski, E. Grodzicka, Z. Gołacki and R. R. Gałązka, *Phys. Rev. Lett.*, 1996, **77**, 3447.
86 S. Isber, C. Fau, S. Charar, M. Averous and Z. Golacki, *Mater. Sci. Forum*, 1995, **182–184**, 657.
87 A. Ishida, T. Tsuchiya, T. Yamada, D. Cao, S. Takaoka, M. Rahim, F. Felder and H. Zogg, *J. Appl. Phys.*, 2010, **107**, 123708.
88 A. Krost, B. Harbecke, R. Faymonville, H. Schlegel, E. J. Fantner, K. E. Ambrosch and G. Bauer, *J. Phys. C: Solid State Phys.*, 1985, **18**, 2119.
89 D. L. Partin, *J. Electron. Mat.*, 1993, **12**, 917.
90 V. Jovovic, S. J. Thiagarajan, J. West, J. P. Heremans, T. Story, Z. Golacki, W. Paszkowicz and V. Osinniy, *J. Appl. Phys.*, 2007, **102**, 043707.
91 X. Gratens, S. Charar, M. Averous, S. Isber, J. Deportes and Z. Golacki, *Phys. Rev. B: Condens. Matter*, 1997, **56**, 8199.
92 P. Norton and M. Tacke, *J. Cryst. Growth*, 1987, **81**, 405.
93 H. Kanazawa, S. Adachi, T. Yamaguchi, S. Murashige and K. Murakami, *J. Appl. Phys.*, 1999, **86**, 2611.
94 F. Geist, W. Herbst, C. Mejia-Garcia, H. Pasher, R. Rupprecht, Y. Ueta, G. Springholtz, G. Bauer and M. Tacke, *Phys. Rev. B: Condens. Matter*, 1997, **56**, 13042.
95 T. Story, M. Górska, A. Łusakowski, M. Arciszewska, W. Dobrowolski, E. Grodzicka, Z. Gołacki and R. R. Gałazka, *Phys. Rev. Lett.*, 1996, **77**, 3447.

96 E. P. Skipetrov, N. A. Chernova and E. I. Slyn'ko, *Phys. Rev. B: Condens. Matter*, 2002, **66**, 085204.
97 H. Preier, *Appl. Phys.*, 1979, **20**, 189.
98 A. J. Rosenberg and F. Wald, *J. Phys. Chem. Solids*, 1965, **26**, 1079.
99 A. A. Averkin, V. I. Kaidanov and R. B. Melnik, *Sov. Phys. Semicond.*, 1971, **5**, 75.
100 B. A. Akimov, R. S. Vadnkhva, V. P. Zlomanov, L. I. Ryabova and S. M. Chudinov, *Sov. Phys. Semicond.*, 1977, **11**, 637.
101 B. A. Akimov, N. B. Brandt, S. A. Bogosloovskii, L. I. Ryabova and S. M. Chudinov, *JETP Lett.*, 1979, **29**, 9; B. A. Akimov, N. B. Brandt, S. O. Klimonskiy, L. I. Ryabova and D. R. Khokhlov, *Phys. Lett. A*, 1982, **88**, 483.
102 V. I. Kaidanov, S. A. Nemov and Yu. I. Ravich, *Sov. Phys. Semicond.*, 1992, **2**, 113.
103 V. I. Kaidanov and Yu. I. Ravich, *Sov. Phys. Usp.*, 1985, **28**, 31.
104 C. M. Jaworski, B. Wiendlocha, V. Jovovic and J. P. Heremans, *Energy Environ. Sci.*, 2011, **4**, 4155.
105 Y. Matsushita, H. Blum, T. H. Geballe and I. R. Fisher, *Phys. Rev. Lett.*, 2005, **94**, 157002.
106 A. S. Ericson, N. P. Breznay, E. A. Nowadnick, T. H. Geballe and I. R. Fisher, *Phys. Rev. B: Condens. Matter Mater. Phys.*, 2010, **81**, 134521.
107 K. Hoang and S. D. Mahanti, private communications.
108 A. N. Veis, S. A. Nemov, V. A. Polovinkin and Yu. l. Ukhanov, *Sov. Phys. Semicond.*, 1977, **11**, 588.
109 V. I. Kaidanov, R. B. Melnik and N. V. Germanas, *Sov. Phys. Semicond.*, 1972, **6**, 627.
110 G. S. Bushmarina, B. F. Gruzinov, I. A. Drabkin, E. Ya. Lev and V. M. Yuneev, *Sov. Phys. Semicond.*, 1984, **18**, 1374.
111 J. O. Dimmock, I. Melngailis and A. J. Strauss, *Phys. Rev. Lett.*, 1966, **16**, 1193.
112 B. A. Akimov, R. S. Vadnkhva, V. P. Zlomanov, L. I. Ryabova and S. M. Chudinov, *Sov. Phys. Semicond.*, 1977, **11**, 637.
113 S. N. Lykov, Yu. I. Ravich and I. A. Chernik, *Sov. Phys. Semicond.*, 1977, **11**, 1016.
114 S. Takaoka, T. Itoga and K. Murase, *Jpn. J. Appl. Phys.*, 1984, **23**, 216.
115 V. Jovovic, S. J. Thiagarajan, J. P. Heremans, T. Kommisarova, D. Khokhlov and A. Nicorici, *J. Appl. Phys.*, 2008, **103**, 053710.
116 B. A. Akimov, L. I. Ryabova, O. B. Yatsekno and S. M. Chudinov, *Sov. Phys. Semicond.*, 1979, **13**, 441.
117 R.-H. Hong, J. D. Dow, O. F. Sankey and R. S. Allgaier, *Appl. Phys. Lett.*, 1996, **68**, 2696.
118 *Landolt-Bornstein Numerical Data and Functional Relationships in Science and Technology*, ed. O. Madelung, Springer-Verlag, Berlin, 1983, vol. 17, Subvol. f; the integrated density-of-states mass is the density of states mass of each pocket of the Fermi surface, multiplied by the number of pockets to the power 2/3.
119 Y. Matsushita, P. A. Wianecki, A. T. Sommer, T. H. Geballe and I. R. Fisher, *Phys. Rev. B: Condens. Matter Mater. Phys.*, 2006, **74**, 134512.
120 H. Kohler, *Phys. Status Solidi B*, 1976, **74**, 591.
121 V. A. Kulbachinskii, N. B. Brandt, P. A. Cheremnykh, S. A. Azou, J. Horak and P. Lostak, *Phys. Status Solidi B*, 1988, **150**, 237.
122 V. A. Kulbachinskii, M. Inoue, M. Sasaki, H. Negishi, W. X. Gao, K. Takase, Y. Giman, P. Lostak and J. Horak, *Phys. Rev. B: Condens. Matter*, 1994, **50**, 16921.
123 V. A. Kulbachinskii, H. Negishi, M. Sasaki, Y. Giman, M. Inoue, P. Losták and J. Horák, *Phys. Status Solidi B*, 1997, **199**, 505.
124 M. K. Zhitinskaya, S. A. Nemov and T. E. Svechnikova, *Proc. 16th International Conference on Thermoelectricity*, IEEE, 1997, p. 97.
125 The thermopower of Bi_2Te_3 is anisotropic in general, but the partial thermopowers of each electron or hole pocket of the Fermi surface are scalars. The anisotropy arises from the fact that the total thermopower is an average of the partial coefficients of each pocket weighted by the partial conductivities of those pockets, which are anisotropic. In degenerately-doped material, all pockets are degenerate, and the thermopower equals the partial hole thermopower of a pocket.
126 G. Bergmann, *Z. Natuforsch.*, 1963, **18a**, 1169.
127 T. Plecháček, J. Navrátil, J. Horák and P. Lošťák, *Philos. Mag.*, 2004, **84**, 2217.
128 P. Hohenberg and W. Kohn, *Phys. Rev.*, 1964, **136**, B864.
129 W. Kohn and L. J. Sham, *Phys. Rev.*, 1965, **140**, A1133.
130 S. Ahmad, K. Hoang and S. D. Mahanti, *Phys. Rev. Lett.*, 2006, **96**, 056403.
131 S. K. Hoang, D. Mahanti and M. G. Kanatzidis, *Phys. Rev. B: Condens. Matter Mater. Phys.*, 2010, **81**, 115106.
132 K. Hoang and S. D. Mahanti, *Phys. Rev. B: Condens. Matter Mater. Phys.*, 2008, **78**, 085111.
133 Yu. I. Ravich and S. A. Nemov, *Semiconductors*, 2002, **36**, 3.
134 A. Bansil, S. Kaprzyk, P. E. Mijnarends and J. Tobola, *Phys. Rev. B: Condens. Matter*, 1999, **60**, 13396.
135 T. Stopa, S. Kaprzyk and J. Tobola, *J. Phys.: Condens. Matter*, 2004, **16**, 4921.
136 S. Kaprzyk and A. Bansil, *Phys. Rev. B: Condens. Matter*, 1990, **42**, 7358.
137 H. Ebert, D. Ködderitzsch and J. Minár, *Rep. Prog. Phys.*, 2011, **74**, 096501.
138 Calculations performed for the aim of this work. Details of calculations are similar to those in ref. 104, where the inaccuracy of the calculation of the gap of PbTe is also discussed.
139 $S(n)$ was calculated with $\lambda = 0$, $E_F = 150$ meV, and eqn (7) in ref. 104; the results here are more accurate, using $\lambda = -0.5$, $E_F = 60$ meV, and eqn (8).
140 E. A. Zvereva, E. P. Skipetrov, O. A. Savelieva, N. A. Pichugin, A. E. Primenko, E. I. Slyn'ko and V. E. Slyn'ko, *J. Phys.: Conf. Ser.*, 2010, **200**, 062039.
141 KKR calculated value of local magnetic moment on Ti is equal to 1.8 μB. The question is if it leads to ferromagnetic ordering when Ti concentration is very small, below 1% in experiment will be addressed to future study.

 This journal is © The Royal Society of Chemistry 2012